In presenting this dissertation as a partial fulfillment of the requirements for an advanced degree from the Georgia Institute of Technology, I agree that the Library of the Institution shall make it available for inspection and circulation in accordance with its regulations governing materials of this type. I agree that permission to copy from, or to publish from, this dissertation may be granted by the professor under whose direction it was written, or, in his absence, by the Dean of the Graduate Division when such copying or publication is solely for scholarly purposes and does not involve potential financial gain. It is understood that any copying from, or publication of, this dissertation which involves potential financial gain will not be allowed without written permission.

Ben Gray Christopher

UNSTEADY FLOW IN A SMOOTH PIPE AFTER INSTANTANEOUS OPENING OF A DOWNSTREAM VALVE

Part I. Mean Flow Characteristics - Velocity

A THESIS

Presented to

the Faculty of the Graduate Division

Georgia Institute of Technology

In Partial Fulfillment
of the Requirements for the Degree
Master of Science in Civil Engineering

by

Ben Gray Christopher

December 1955

3 1
12K

UNSTEADY FLOW IN A SMOOTH PIPE AFTER INSTANTANEOUS OPENING OF A DOWNSTREAM VALVE

Part I. Mean Flow Characteristics - Velocity

Approved:

Date Approved by Chairman: Dec. 29, 1955

ACKNOWLEDGMENTS

The writer wishes to thank all persons who made this thesis possible. This thesis is a part of a study sponsored by the National Science Foundation. Dr. M. R. Carstens was the director of this study and acted in the capacity of thesis advisor. The writer is deeply indebted to Dr. Carstens for his valuable guidance and assistance in this work. The other members of the thesis reading committee were Professors C. E. Kindsvater and G. W. Rainey.

Mr. J. B. Trimble participated in this study and was a co-worker to the fullest extent in the experimental portion of this work. Acknowledgment is also given to Mr. J. E. Roller for his criticisms and for his help in the construction of the equipment. Mr. H. J. Bates, hydraulic lab technician, gave suggestions and assistance in the construction of the experimental equipment. This thesis was typed by Mrs. Martha McCalla.

TABLE OF CONTENTS

LIST OF FIGURES

LIST OF FIGURES (continued)

LIST OF TABLES

SUMMARY

An experimental study was performed in order to determine the mean flow characteristics in a pipe during flow establishment. The smooth, straight, circular pipe was horizontally aligned. The upstream extremity of this pipe was a well-rounded inlet which was located in a large reservoir. The downstream extremity of this pipe was unobstructed so that a liquid jet was formed in the atmosphere downstream from the pipe outlet. Velocity-time data were obtained from a motion picture record of the jet. Pressure-time data were obtained at selected points along the pipe. These data were recorded by sending the output signals of pressure transducers through an oscillograph.

The experiments were performed with a systematic variation of the independent dimensionless variables. These independent dimensionless variables were pipe length to pipe diameter ratio L/D and an inertial reaction to viscous shear force ratio $gh_oD^3/L\nu^2$. h_o is the piezometric head in the reservoir and ν is the kinematic viscosity of the fluid. The value of L/D was established at 95, 190, 285, 380, and 475. The value of $gh_oD^3/L\nu^2$ was established at $6(10^6)$, $12(10^6)$, $18(10^6)$, $24(10^6)$, and $30(10^6)$. Thus the total number of experimental runs was twenty-five.

Supplementary analysis was required in order to determine the mean velocity in the pipe from the motion picture record of the jet. As the result of the action of shear forces, the velocity distribution is non-uniform. Consequently the jet issuing from the pipe outlet had greater

linear momentum than if the velocity distribution were uniform. Thus the problem was to determine the non-uniformity of the velocity distribution in order to relate the observed velocity to the mean velocity. During the laminar flow, the velocity was assumed to have a uniform distribution in a central core region and to have a parabolic distribution within the boundary layer region. This boundary layer thickness was determined by three methods which utilized experimental data. During the turbulent flow, the velocity was assumed to have a distribution based on the seventh-root law of velocity distribution.

The observed and the mean velocity-time data are presented in this thesis in the form of various graphs and curves. The pressure-time data are to be presented in Part III of this study. A detailed analysis of the transition from laminar to turbulent flow is presented in Part II of this study.

Significant results obtained from this study are as follows. (1) For turbulent flow conditions, the method of obtaining mean velocities by jet photography entails only an assumption of a velocity distribution. (2) For laminar flow, the method of jet photography for obtaining mean velocities requires that a velocity distribution be assumed, that pressure measurements be obtained at various points along the pipe, and that there be no separation of the issuing laminar jet. (3) Characteristic laminar jet separation will occur if the non-uniformity of the velocity distribution as measured by the ratio of the nominal boundary-layer thickness to the pipe radius exceeds a value of 0.65. (4) The exact variation of velocity with respect to time during flow establishment is a function of

the time of turbulence inception, the rate of growth of the turbulent region, and the position of turbulence inception. (5) The experimental parameters utilized are sufficient to insure similarity in regard to the time of turbulence inception and the rate of growth of the turbulent region. Since the position of turbulence inception is apparently random, the experimental parameters are not sufficient to insure exact similarity in regard to the variation of velocity with respect to time during flow establishment. (6) The use of step computation methods employing a variable value of the Darcy-Weisbach f is unwarranted in practical engineering solutions utilizing one-dimensional methods of analysis. The use of a constant value of f is sufficiently accurate.

CHAPTER I

INTRODUCTION

The mean flow characteristics --boundary shear stress, velocity distribution, and total energy changes-- of steady flow in both rough and smooth pipes have been extensively studied by experimental and mathematical methods. The validity of the solution to the Navier-Stokes equations for a long, straight, circular conduit was verified experimentally by the middle of the nineteenth century. This solution is known as the Hagen-Poiseuille equation and is valid as long as the flow is laminar. Steady turbulent flow in a pipe is of greater significance to the engineer, but the mathematical solution for this type of flow has not been obtained because of the complexity of the turbulence associated with the motion. Nevertheless, the importance of determining the mean flow characteristics of steady turbulent flow is related to the vast number of reported experimental studies. The experiments prior to the twentieth century were limited in scope and were reported as empirical equations. Rational analysis of the mean flow characteristics of steady turbulent flow has been progressively improved by many workers, with the most notable advances being made by Reynolds, Prandtl, and Von Kármán. The classic experiments of Nikuradse in conjunction with the analyses of Prandtl and Von Kármán are the basis of satisfactory rational expressions for the mean flow characteristics except in the

transition region from the hydraulically smooth pipe to the hydraulically rough pipe.

The detailed turbulent flow characteristics in a pipe have not been subjected to rational analysis and have only recently been the object of experimental research. The statistical theory of turbulence is useful mainly as an experimental tool. The statistical theory is indicative of the quantities that must be measured, that is, scale, intensity, and correlation coefficients. This theory is of very limited utility for explaining the observed turbulence characteristics and for relating these turbulence characteristics and the boundary conditions. Because of the difficult experimental techniques involved, reported experimental research is both limited and recent [1], [2].

If the subject of pipe flow is extended to include unsteady flow, one finds that the reported works concerning unsteady flow are divided into two categories. The first category includes a vast amount of literature presenting methods of analysis for specific problems [3], for example, the methods employed in the design of a surge tank at a hydroelectric installation. Invariably, these analyses are based upon the use of the steady flow boundary shear stress. The second category includes a limited amount of literature in which the mean flow characteristics of unsteady flow are determined without utilizing the steady flow characteristics. Unsteady laminar flow in a U tube has been investigated by Valensi and Clarion [4], Clarion [5], Yanada and Taneda [6], and Christopherson [7]. Jones [8] investigated oscillatory laminar motion in a straight tube. These investigations were for the purpose of

determining boundary shear stress. A more limited experimental study to determine the velocity distribution of laminar flow starting from rest in a straight circular tube was performed by Crausse [9]. Boundary shear stress determinations in unsteady turbulent flow were experimentally obtained in a straight pipe by Daily and Deemer [10]. To the writer's knowledge there have been no studies concerning the detailed turbulence characteristics of unsteady pipe flow.

The paucity of information concerning unsteady flow in pipes can be traced to three causes. In the first place, the study of steady flow in pipes has been a fruitful field of research. Being a simpler and more common flow condition, it is natural and proper that greater efforts would be devoted to steady flow studies. In the second place, the instrumentation for unsteady flow is more complex; the study requires rapid time response instruments which are only now becoming readily available. In the third place, the boundary conditions apart from geometrical boundary conditions are infinite in number. For example, the mean flow characteristics of laminar flow would be different for oscillation in a straight tube and for flow establishment in a straight tube. Thus, the instantaneous flow characteristics of unsteady laminar flow will depend upon the history or the aggregate of past events of that flow. Fortunately, the flow characteristics of unsteady turbulent pipe flow can be expected to be independent of the history of the motion.

In view of the extremely limited number of studies concerning the flow characteristics in unsteady flow, the selection of a particular problem is not guided by past experiments, but primarily by the amount

of information that can be obtained from a limited study. In the first place, the problem should be of technical interest. In the second place, it is desirable to have unsteady turbulent flow since the results do not depend upon the history of the motion and thus these results will be more generally applicable. The problem of flow establishment in a straight circular pipe attached to a large reservoir was judged to be a problem worthy of study in view of the above standards.

An experimental study of the mean flow characteristics during flow establishment was performed in the Hydraulics Laboratory of the Georgia Institute of Technology. A straight circular pipe was horizontally aligned. The upstream extremity of this pipe was placed in a large reservoir. The downstream extremity was unobstructed so that a free jet was formed in the atmosphere downstream from the pipe. The flow was established by instantaneous release of a disk valve placed against the square-edged downstream end of the pipe. Velocity-time data were obtained from a motion-picture record of the jet. Pressure-time data were obtained at selected points along the pipe.

From the results of this experiment, mean flow characteristics can be determined in both laminar and turbulent flow. In addition to the general sequence of events, the details of the transition from laminar to turbulent flow can also be observed. The complete report of the experimental program and results is to be contained in three master's theses as follows:

UNSTEADY FLOW IN A SMOOTH PIPE AFTER INSTANTANEOUS OPENING OF A DOWNSTREAM VALVE

Part I. "Mean Flow Characteristics-Velocity," by B. G. Christopher;

Part II. "Transition from Laminar to Turbulent Flow," by J. B. Trimble; and

Part III. "Mean Flow Characteristics-Pressure and Boundary Shear," by J. E. Roller.

The report of the mathematical investigation of this problem is contained in one master's thesis:

UNSTEADY FLOW IN A SMOOTH PIPE AFTER INSTANTANEOUS OPENING OF A DOWNSTREAM VALVE

Part IV. "Mathematical Analysis," by R. W. Olive.

CHAPTER II

THEORETICAL CONSIDERATIONS

A complete mathematical treatment is not possible for the problem of flow establishment in a straight tube after instantaneous opening of a downstream valve. In the first place, the flow is initially laminar but soon is turbulent. During the initial laminar stage, the solution of the Navier-Stokes equations with the proper boundary conditions would constitute an exact solution for this stage. However, no such exact solution is possible in the later turbulent stage since there are no counterparts in turbulent flow to the Navier-Stokes equations of laminar flow. Even in the initial laminar stage an exact solution of the Navier-Stokes equations has not been obtained since pressure, boundary shear, and velocity are a function of distance from the inlet as well as time. Even though no exact solution for this problem is available, solutions of allied problems, approximate solutions, and the differential equations are invaluable in organizing and analyzing experimental data.

Related solutions of the Navier-Stokes equations.—Szymanski [11] obtained a solution of the Navier-Stokes equations for flow establishment in a straight tube, assuming that the pressure gradient is a constant. For two reasons this solution is only remotely related to the flow resulting from instantaneous opening of a downstream valve in a straight

pipe attached to a large reservoir. First, as a result of utilizing a constant pressure gradient, the effects of the inlet are not incorporated. In other words, the solution is independent of the coordinate of distance from the inlet. In the physical problem, the values of the pressure gradient, the point velocity, and the boundary shear stress are all influenced by the proximity of the inlet. This inlet region or region of appreciable influence is not static but is continuously enlarged with the passage of time. Second, the pressure at the inlet end of the pipe changes continuously with time even though the upstream reservoir is large and the potential energy of the fluid in the reservoir is constant. This pressure must be lower than the reservoir piezometric pressure in order to accelerate the fluid to the inlet. Consequently the pressure will be lower at the inlet not only by the amount of potential energy converted to kinetic energy but by an amount that is related to the local acceleration. Thus the Szymanski solution can be only of qualitative interest in connection with the developing velocity profiles with time.

Langhaar [12] obtained an approximate solution of the Navier-Stokes equations in the region downstream from a streamlined inlet for the case of steady flow. This solution is of qualitative interest in connection with the developing velocity profiles with distance from the inlet.

In Part IV of this study, Olive obtained a solution of the Navier-Stokes equations for the case in which the pressure gradient varies linearly with time but is independent of the distance coordinate from

the inlet. Obviously, this solution does not include any effects due to the inlet region. Also, the utilization of a pressure gradient that varies linearly with time is only an approximation. Nevertheless, the solution should be a reasonable facsimile of the physical conditions at small values of time when the inlet region is short in relation to the total pipe length.

One-dimensional analysis.---Gross simplification of the problems can be made by utilizing the methods of one-dimensional analysis. The two fundamental concepts of one-dimensional analysis are as follows: (1) the piezometric pressure or piezometric head is constant in a cross section which is normal to the direction of flow; and (2) the various point velocities can be replaced by the mean velocity V in the cross section. This second concept is directly applicable in the equation of continuity for the total cross section. In order to apply the second concept to the energy equation it is necessary to multiply the kinetic energy based on the mean velocity by the kinetic energy correction factor K_e in order to obtain the true mean kinetic energy. In a like manner, the linear momentum flux based on the mean velocity must be multiplied by the momentum correction coefficient K_m in order to obtain the true linear momentum flux.

Prior to applying one-dimensional analysis to the pipe section, an approximate analysis is presented to evaluate the pressure at the pipe inlet. Figure 1 is a definitive sketch of irrotational flow into a rounded inlet. The flow is presumed to approach the inlet in a manner

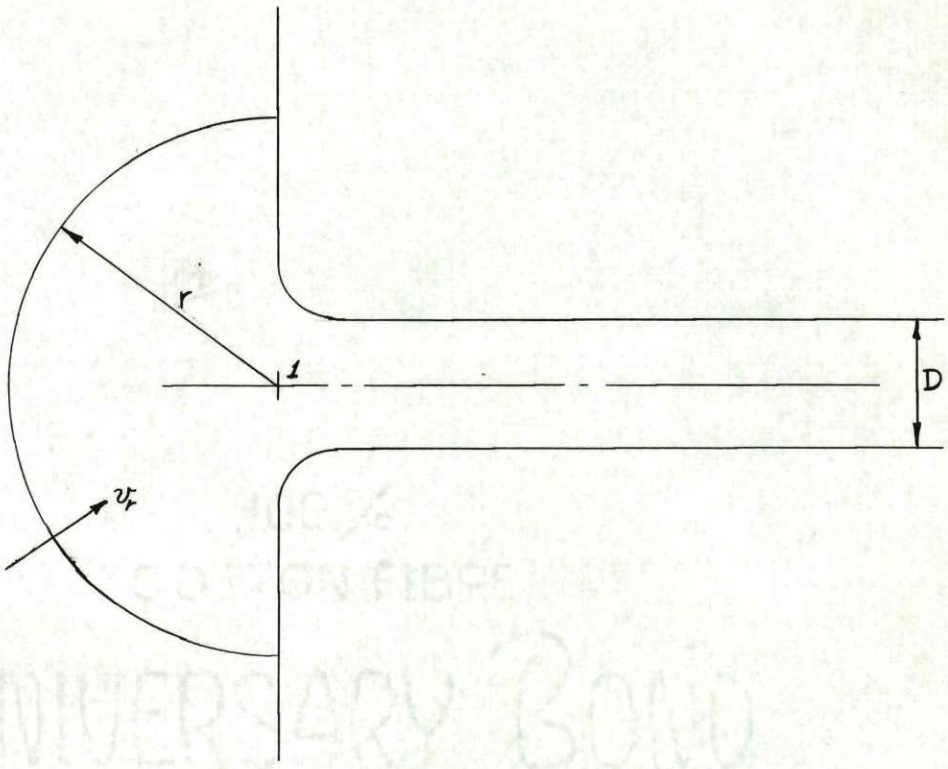

Fig. 1. Flow into a rounded inlet

similar to the three-dimensional hydrodynamic sink; that is, the velocity is entirely in the radial direction, the velocity-potential surfaces are hemispherical, and the velocity magnitude is constant on each potential surface. With an incompressible fluid, the volume rate of flow Q past every normal section is a function only of time. Thus the equation of continuity can be written in the following forms,

$$Q = VA = V \frac{D^2 \pi}{4} \tag{1}$$

and

$$Q = - v_r \, 2 \pi r^2 \tag{2}$$

in which V is the mean velocity in the pipe, D is the pipe diameter, r is the radial coordinate of the sink, and v_r is the velocity in the field of the sink. Thus,

$$v_r = - \frac{D^2}{8r^2} V \tag{3}$$

and

$$\frac{\partial v_r}{\partial t} = - \frac{D^2}{8r^2} \frac{dV}{dt} \tag{4}$$

Since the shear will be negligible in the sink field, the equation of motion is

$$- \frac{\partial p}{\partial r} = \rho v_r \frac{\partial v_r}{\partial r} + \rho \frac{\partial v_r}{\partial t} \tag{5}$$

in which ρ is the fluid density and p is the piezometric pressure. Substituting Eq. (4) in Eq. (5) and taking the dot product with dr, the differential work-energy equation is derived.

$$- \frac{\partial}{\partial r} \left[\rho \frac{v_r^2}{2} + p \right] \cdot dr = \rho \frac{D^2}{8} \frac{dV}{dt} \frac{1}{r^2} \cdot dr \tag{6}$$

The indicated integration is performed with the following limits as $r \longrightarrow \infty$, $v_r \longrightarrow 0$, and $p \longrightarrow p_o$ in which p_o is the piezometric pressure in the large reservoir. The lower limit of r is $D/\sqrt{8}$ or the position at which $|v_r| = |V|$. The result is

$$p_1 = p_o - \rho \frac{V^2}{2} - \rho \frac{D}{\sqrt{8}} \frac{dV}{dt} \tag{7}$$

It is apparent from Eq. (7), that the entire effect of unsteadiness in the motion is contained in the third term on the right $\rho (D/\sqrt{8})\ (dV/dt)$.

The differential equation and the solution are readily obtained for flow establishment in a straight pipe attached to a large reservoir if boundary shear stress is neglected and one-dimensional analysis are employed. Figure 2 is a definitive sketch for flow in a straight pipe attached to a large reservoir.

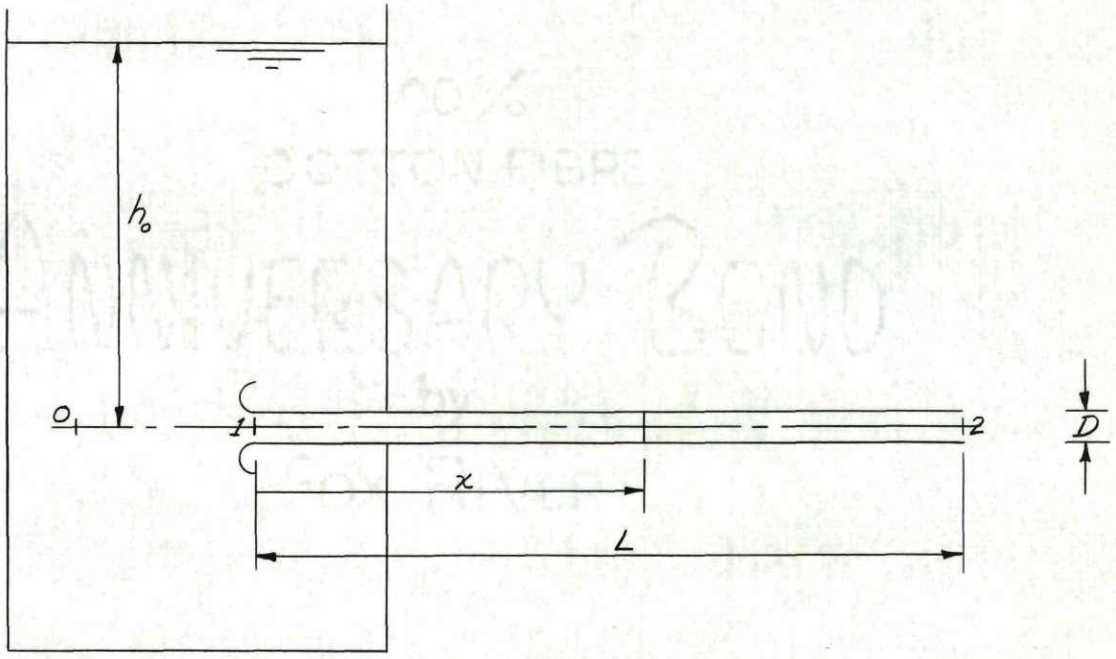

Fig. 2. Flow in a straight pipe attached to a large reservoir

The differential equation for this case is simply

$$-\frac{\partial p}{\partial x} = \rho \frac{dV}{dt} \tag{8}$$

The pressure gradient is assumed to be a function of time only; that is, the inlet region effects are neglected. The pressure p_2 at the outlet

is atmospheric and is arbitrarily established at a zero value. Thus

$$-\frac{\partial p}{\partial x} = \frac{p_1 - p_2}{L} = \frac{p_1}{L} \tag{9}$$

Substituting Eqs. (7) and (9) in Eq. (8) a separable differential equation is obtained. The solution of this equation is

$$\frac{V}{\sqrt{2gh_o}} = \tanh\left[\frac{1}{\sqrt{2}}\,\frac{\sqrt{gh_o}\,t}{L}\right]\left[\frac{\sqrt{8}\,(L/D)}{1+\sqrt{8}\,(L/D)}\right] \tag{10}$$

Utilizing the same assumptions as used in the derivation of Eq. (10) the effect of boundary shear can be incorporated. The differential equation corresponding to Eq. (8) for this case is

$$-\frac{\partial p}{\partial x} - \frac{4\,\tau_o}{D} = \rho\frac{dV}{dt} \tag{11}$$

in which τ_o is the boundary shear stress. Assuming that τ_o is a function only of time and that the magnitude of the shear stress is identical to the steady-state shear stress, it follows that

$$\tau_o = \frac{f}{8}\,\rho\,V^2 \tag{12}$$

in which f is the steady-state Darcy-Weisbach friction factor. Equation (12) is then substituted in Eq. (11). The derivation and solution parallel that given in the preceding paragraph. The only difference arises because, with the inclusion of boundary shear, the velocity distribution across the pipe may not be uniform. Hence, the only change involved is that the multiplier of the kinetic energy term in Eq. (7) is no longer

unity but is K_e. The resulting solution is readily obtained analytically if it is further assumed that f is a constant; otherwise, the solution must be obtained by numerical methods. Assuming f is a constant, it follows that

$$\frac{V}{\sqrt{2gh_o}} = \frac{\tanh\left[\frac{1}{\sqrt{2}}\ \frac{\sqrt{gh_o}\,t}{L}\right]\left[\sqrt{K_e + \frac{fL}{D}}\right]\left[\frac{\sqrt{8}(L/D)}{1+\sqrt{8}(L/D)}\right]}{\sqrt{K_e + \frac{fL}{D}}} \tag{13}$$

Inasmuch as the boundary shear was neglected in the derivation of Eq. (10) and the boundary shear was overestimated in the derivation of Eq. (13), the experimental values will be intermediate between these two functions.

The complete one-dimensional differential equation of motion is of value in the determination of boundary shear from experimentally determined values of pressure and velocity. The fluid element utilized in the derivation is a cross sectional element of the fluid in the pipe which is dx in length.

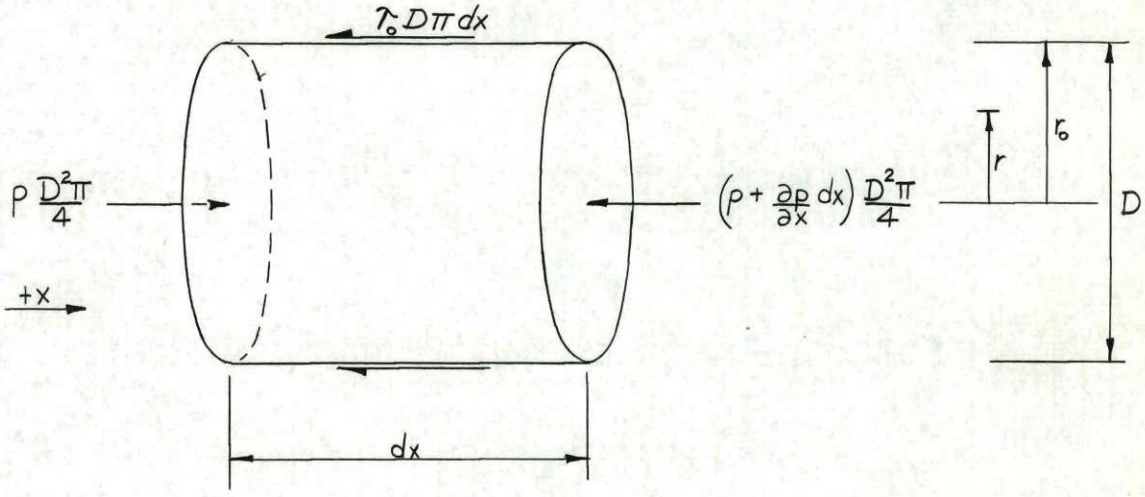

Fig. 3. Fluid element within the pipe

The external forces on the fluid element in the x direction are the resultant pressure force on the end areas and the boundary shear force. The momentum equation for this element is

$$-\frac{\partial p}{\partial x}\,dx\,\frac{D^2\pi}{4} - \gamma_o D\,\pi\,dx = \frac{\partial}{\partial x}\left[\int_A \rho\,v\,dQ\right]dx + \frac{\partial}{\partial t}\int_{\forall} \rho\,v\,d\forall \qquad (14)$$

The first term on the right side of Eq. (14) is the difference of momentum flux through the end areas of the fluid element. Utilizing the one-dimensional method,

$$\int_A \rho\,v\,dQ = K_m \rho Q V = K_m \rho V^2 \frac{D^2\pi}{4} \qquad (15)$$

The second term on the right side of Eq. (14) is the time rate of change of linear momentum of the particles on the interior of the element. The symbol $\forall$ is used to represent volume.

$$d\forall = dA\,dx$$

The end areas of the element are chosen so that dx is a constant for every dA. Thus,

$$\frac{\partial}{\partial t}\int_{\forall} \rho\,v\,dV = \frac{\partial}{\partial t}\left[\int_A \rho\,v\,DA\right]dx = \rho\frac{\partial Q}{\partial t}\,dx. \qquad (16)$$

Since,

$$Q = V\,A$$

and since Q is function of time alone

$$\frac{\partial Q}{\partial t} = \frac{D^2\pi}{4}\frac{dV}{dt} \qquad (17)$$

Introducing Eqs. (15), (16), and (17) into Eq. (14) and dividing by the elemental volume, the desired differential equation is

$$-\frac{\partial p}{\partial x} - \frac{4\tau_o}{D} = \rho V^2 \frac{\partial K_m}{\partial x} + \rho \frac{dV}{dt} \qquad (18)$$

By means of Eq. (18), the boundary shear can be determined in turbulent flow regions where $\partial K_m / \partial x = 0$, provided that experimentally determined values of $\partial p / \partial x$ and dV/dt are available. Evaluation of boundary shear is discussed in detail in Part III of this study. Also Eq. (18) is invaluable in the determination of laminar flow velocity distribution characteristics from measured values of $\partial p / \partial x$ and dV/dt. Velocity distribution is discussed in detail in the following section and in Chapter IV, EXPERIMENTAL RESULTS.

Boundary layer analysis.--Details of laminar velocity distribution are readily visualized by employing the boundary layer concept. The boundary layer is conceived as being the region adjacent to the boundary in which the effects of shear predominate. Conversely, the region outside the boundary layer is not influenced by the boundary shear. With the flow separated into these two regions, different analyses may be advantageously applied in each region. Boundary layer analysis is not ordinarily associated with steady pipe flow since the boundary layer extends to the pipe centerline. Two examples of pipe flow in which the boundary layer does not extend to the pipe centerline are (1) following a streamlined pipe inlet in the region of a spatially developing velocity profile and (2) during the time of flow establishment with a chronologically

developing velocity profile. A successful analysis of the first of these flow situations was performed by Schiller [13] utilizing uncomplicated boundary layer concepts.

Schiller studied the developing laminar velocity profile downstream from a streamlined inlet for steady pipe flow. A uniform velocity distribution was assumed immediately downstream from the inlet. At some distance downstream from the inlet the velocity distribution approaches the parabolic velocity distribution. Schiller assumed a boundary layer region with parabolic velocity distribution and a core region of uniform velocity distribution as shown on Fig. 4. By choosing the parabolic velocity distribution within the boundary layer, the parabolic velocity distribution in the pipe is attained at the point where the boundary

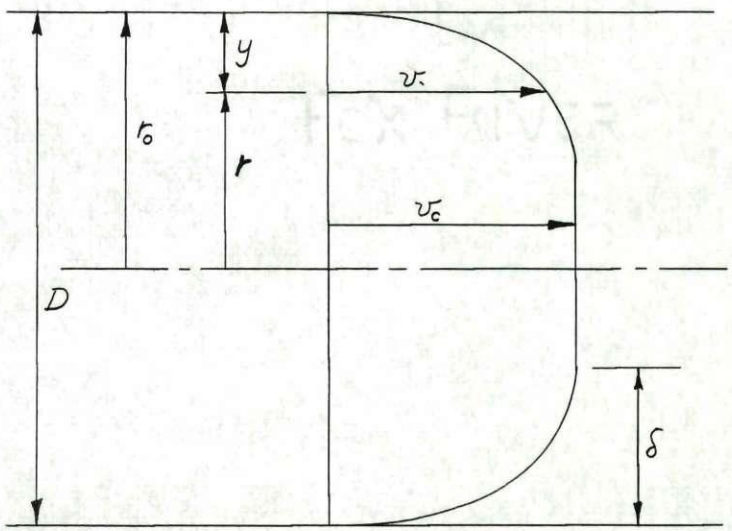

Fig. 4. Laminar boundary layer after Schiller

layer thickness δ is equal to the pipe radius r_o. Schiller utilized this boundary layer in the one-dimensional equations of motion and

obtained a solution for the spatial development of the boundary layer. Velocity measurements by Nikuradse [13] in this region were in surprisingly good agreement with the Schiller solution. Since the boundary layer with parabolic velocity distribution was found to be a good approximation for the spatially developing layer, the employment of the parabolic velocity distribution in the laminar boundary layer is suggested for the case of the chronologically developing layer.

The experimental measurements of Crausse [9] are indicative that the chronologically developing boundary layer in a pipe after flow establishment can be closely approximated by the Schiller velocity profile. Crausse determined the point velocities in a pipe during flow establishment by measuring trajectories of suspended aluminum particles. Crausse photographed the aluminum particles at a point which was sixty diameters from the reentrant inlet from a large reservoir. A sharp-edged orifice was placed at the downstream end of the straight circular tube. The measured point velocities are shown on Fig. 5. The upper one-half of Fig. 5 is a comparison of the chronologically developing velocity profile between the Crausse data and the Szymanski [11] solution. The Szymanski solution was obtained by assuming a constant value of the pressure gradient. With the physical arrangement of Crausse's experiment the magnitude of the pressure gradient was decreasing with time. This difference is reflected in a more rapidly developing velocity profile in the experiments. The lower one-half of Fig. 5 merely illustrates that Crausse's experimentally determined velocity profiles can be approximated by the Schiller velocity profiles.

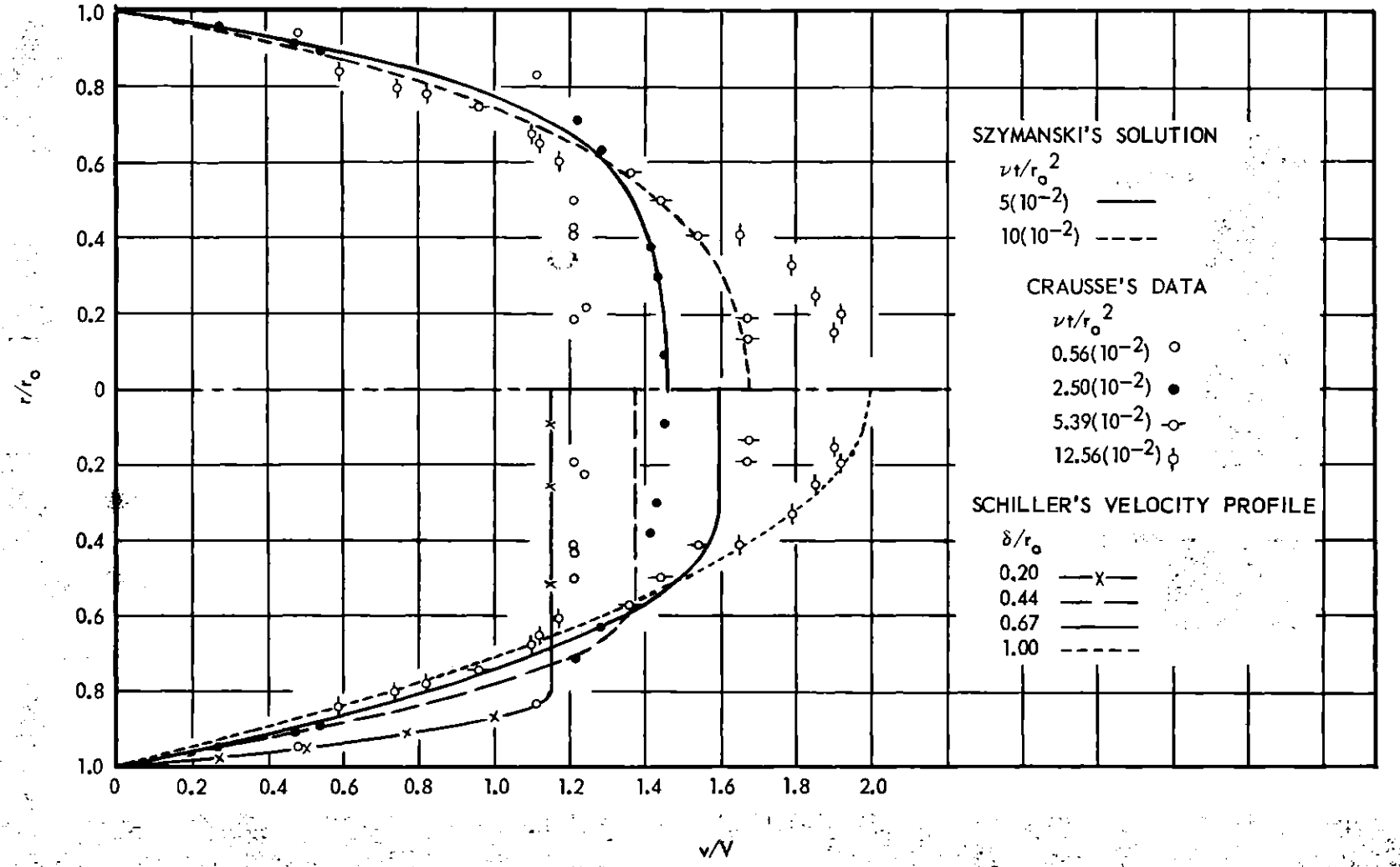

Figure 5. Comparison of velocity distributions.

The Schiller velocity profile is

$$v = v_c = \text{constant} \tag{19}$$

within the central core region and

$$v = v_c \left[2 \frac{y}{\delta} - \left(\frac{y}{\delta} \right)^2 \right] \tag{20}$$

within the laminar boundary layer in which y is the distance from the pipe wall (Fig. 4). The mean velocity V is

$$V = v_c \left[\frac{6-4n + n^2}{6} \right] \tag{21}$$

in which $n = \delta/r_o$. The boundary shear stress τ_o is

$$\tau_o = \frac{1}{n} \left[\frac{6}{6-4n + n^2} \right] \frac{4\mu V}{D} \tag{22}$$

in which μ is the dynamic viscosity of the fluid. The values of one-dimensional momentum and kinetic energy correction coefficients are functions only of the velocity profile and not the velocity magnitude. Hence, the linear momentum correction coefficient K_m and the kinetic energy correction coefficient K_e are functions of the dimensionless boundary layer thickness n.

$$K_m = \left[\frac{6}{6-4n + n^2} \right]^2 \left[\frac{15-14n + 4n^2}{15} \right] \tag{23}$$

$$K_e = \left[\frac{6}{6-4n + n^2} \right]^3 \left[\frac{140-152n + 47n^2}{140} \right] \tag{24}$$

Utilizing the Schiller velocity profiles, boundary layer growth with time can be determined from experimentally determined pressure gradient-time and velocity-time data during flow establishment. During the time of flow establishment the laminar boundary layer thickness is increasing with time but, in addition, the boundary layer thickness is increasing with increasing distance from the inlet. The region of spatially developing layer thickness is a region of decreasing shear with increasing distance from the inlet in accordance with Eq. (22). This region is also a region of increasing values of K_m with increasing distance from the inlet in accordance with Eq. (23). The combined effect of the increasing value of K_m and the decreasing value of shear with distance results in a pressure gradient with decreasing steepness with increasing distance from the inlet. Thus a region in which the pressure gradient is varying is a region of spatially developing boundary layer thickness and conversely a region in which the pressure gradient is constant is a region of constant boundary layer thickness. Therefore, in a region of constant pressure gradient, the value of $\partial K_m / \partial x$ will be zero. Considering only such a region and introducing Eq. (22) in Eq. (18), it follows that

$$-\frac{\partial p}{\partial x} - \frac{16\mu V}{D^2}\left[\frac{1}{n}\right]\left[\frac{6}{6-4n+n^2}\right] = \rho\frac{dV}{dt} \qquad (25)$$

This expression is the basis for the computation of relative boundary layer thickness from experimentally determined values of $\partial p/\partial x$, V, and dV/dt. The adaptation of Eq. (25) for computational purposes and the results of this computation are presented in Chapter IV, EXPERIMENTAL RESULTS.

CHAPTER III

EXPERIMENTAL PROGRAM

General description of experiment.--Flow establishment in a smooth pipe after instantaneous opening of a downstream valve was studied by means of experimental determination of velocity and pressure as functions of time. During the time of flow establishment, a motion picture was taken of the jet issuing from the pipe outlet. From this film, the variations of velocity with time were determined. Continuous pressure-time measurements were simultaneously taken at different points along the pipe. The pressure-time measurements are to be used primarily in the investigation of shear during flow establishment, but a very important secondary use of these records is in the study of the transition from laminar to turbulent flow. Pressure-time data are to be presented in Part III of this study.

The different variables involved in this problem (Fig. 2) may be divided into three categories: flow, geometry, and fluid properties. The flow variables are: V, the mean velocity; t, the elapsed time from valve opening; and gh_o, the potential energy per unit mass of the fluid. The geometric variables are: L, the pipe length; D, the pipe diameter; and also the rounded inlet, and the smooth pipe. The fluid property variable is ν, the kinematic viscosity of the fluid. Thus,

$$V = f(t, gh_o, L, D, \nu)$$

in which V is the dependent variable and all others are independent. Utilizing dimensional analysis, this functionality may be written in dimensionless terms as

$$\frac{V}{\sqrt{2gh_o}} = f\left[t\,\frac{\sqrt{gh_o}}{L},\ \frac{L}{D},\ \frac{gh_o D^3}{L\upsilon^2}\right]$$

The selection of these particular forms of the dimensionless parameters is indicated by their appearance in the one-dimensional solutions, Eqs. (10) and (13).

The procedure for experimentation was based upon a systematic variation of the above dimensionless parameters. The length parameter, L/D, was varied from approximately 95 to approximately 475 in four equal increments. For each value of L/D, the head parameter, $gh_oD^3/L\upsilon^2$, was systematically varied from the value of 6×10^6 to 30×10^6 in four equal increments. Since $V/\sqrt{2gh_o}$ is a continuous function of $t\sqrt{gh_o}/L$ and since this continuous function was determined in each run, no special measures were required to obtain a systematic variation of the independent variable $t\sqrt{gh_o}/L$. Thus the entire study consisted of 25 runs. A complete tabulation of these runs is presented in Table I, APPENDIX.

Detailed description of equipment.—Figure 6 is a photograph showing an overall view of the equipment used in this study. The description of the equipment components is presented from the upstream section to the downstream.

The reservoir (A, Fig. 6) was a 575-gallon cylindrical steel tank with a diameter of 42 inches. Due to space limitations, a water-stand-

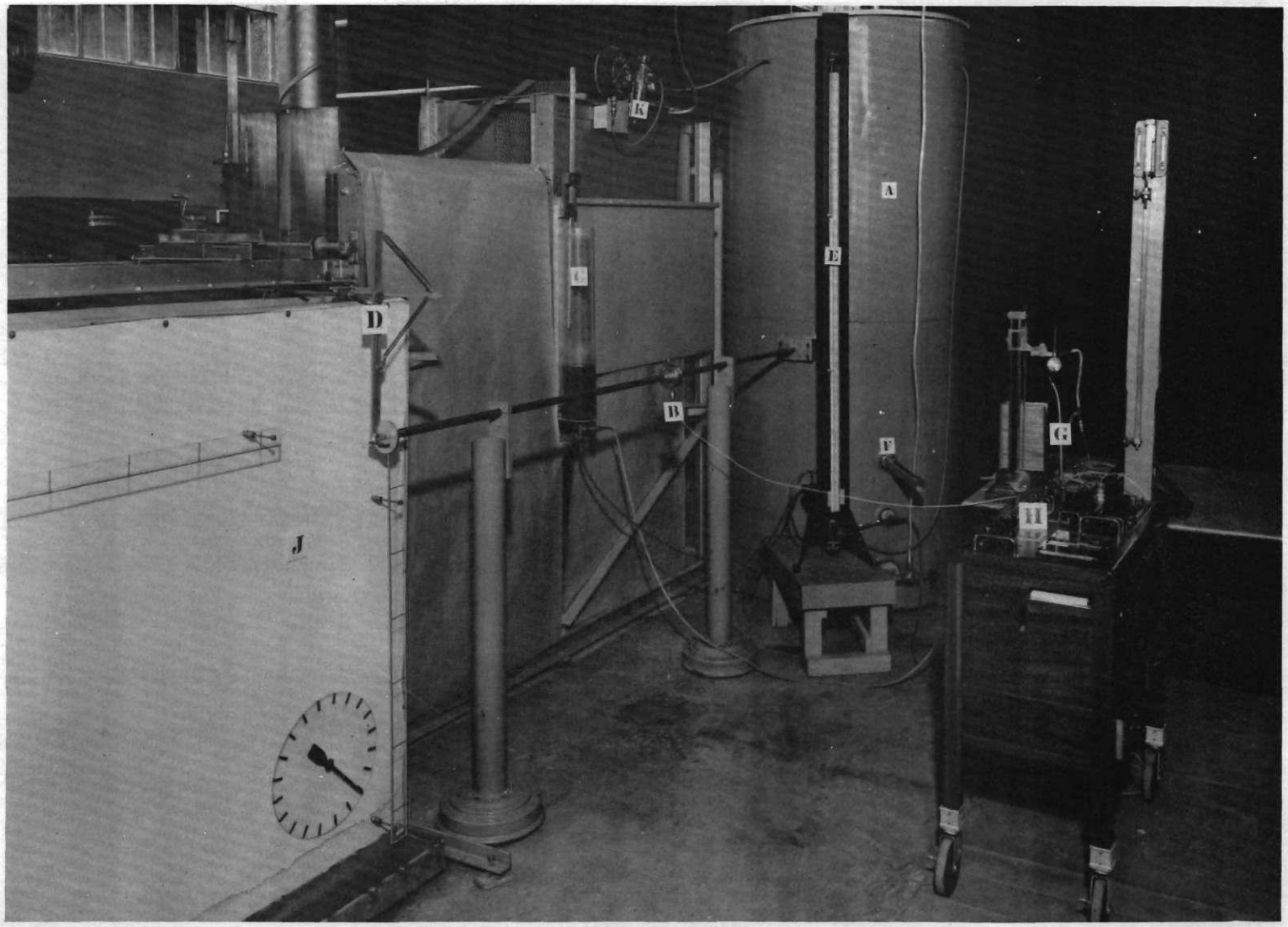

Figure 6. General arrangement of equipment.

pipe air regulator was used to obtain high heads of water without excessive reservoir height (Fig. 7). The tank was sealed and compressed air was introduced into the reservoir in the space above the water level. The flow of air was controlled by a needle valve (Fig. 7 and K, Fig. 6) and the water level in the standpipe was varied to produce the different air pressures required. As long as a small stream of air bubbled from the submerged air line, the air pressure was practically constant throughout the system and was equal to the height of water in the standpipe.

The water level in the reservoir was kept nearly constant by the use of the glass-tubed water level indicator (E, Fig. 6). The water temperature was obtained by a mercury thermometer (F, Fig. 6) located in the side of the reservoir. The thermometer had a range of 0° to 50° centigrade with graduations of 0.1° centigrade.

The total head was measured by means of a water-mercury differential manometer (G, Fig. 6). The centerline of the pipe was used as the manometer reference base, which was obtained by connecting the manometer to the well (C, Fig. 6). The water level in this well (C, Fig. 6) was established at the centerline of the pipe with the aid of the hook gage in the well. Two manometers were used during the tests. The small manometer, with vernier divisions of 0.001 inch, was employed for heads less than twelve feet. The large manometer, with vernier divisions of 0.001 foot, was employed for heads greater than twelve feet. Thus the maximum error in the readings was less than ± 0.15 per cent.

In order to easily and systematically vary the pipe length, five sections of extra-heavy smooth brass pipe were used (Table II, APPENDIX).

Each end of each pipe section was milled on a lathe to fit into the carefully machined brass sleeve coupling which assured axial alignment. Micrometer measurements of the inside diameter of each end of each pipe showed the diameter to be 0.544 ± 0.0005 inches. The pipes proved to be uniform when checked by the method of water-weight and volume-enclosed for each pipe section. The pipes were supported by clamping in adjustable wooden brackets which, in turn, were bolted to heavy-base stands.

The rounded pipe inlet was made of machined brass with the inlet radius of roundness equal to 1.13 pipe diameters. The inlet was attached to the first pipe section by a slip-fit of close tolerance similarly to the sleeve coupling. The inlet was fitted to pipe no. 1 and was carefully scraped with a sharp knife to insure continuity at the junction of pipe wall and inlet. Slightly upstream from the tangent point of inlet roundness, a band of sand roughness approximately 1/8-inch wide was placed around the inlet mouth. The sand gradation used was that which passed the No. 100 screen but was retained on the No. 200 screen.

This experimental study required that a downstream valve be rapidly opened without decelerating or accelerating the oncoming flow. The type of valve selected for this study was a flat aluminum disk faced with a smooth piece of hard-rubber gasket material. The disk valve was located at the end of the downstream pipe section, fitting flush to the pipe end. The valve opening mechanism was a simply supported rotating arm activated by springs (D, Fig. 6). The disk valve was coupled to the rotating arm by means of a ball and socket connection. The primary or accelerating spring produced enough force to give the disk valve a

greater acceleration than was to be encountered by the fluid in the proposed tests. The secondary or resisting spring was strong enough to overcome the primary spring force plus the force due to the water pressure. Rapid valve opening was accomplished within the defined meaning by release of the secondary spring.

The coordinate frame (J, Fig. 6) provided support for the valve, the grid scales, the clock, and the light source for photographing the jet. The coordinate frame consisted of two parallel 53-by 66-inch angle-iron frames, rigidly connected and having four elevating screws in its base. The back frame was covered with a one-half inch plywood board on which the bank of fluorescent back lights was mounted. The bank of lights consisted of ten 40-watt 48-inch (Standard Cool White, Rapid Start) fluorescent lamp tubes placed vertically and spaced at six inches on center. The front frame was covered with a sheet of one-quarter inch thick clear plastic. Immediately behind this plastic sheet a piece of white cotton cloth was smoothly stretched in order to evenly diffuse the transmitted light. The horizontal and vertical coordinate grid scales were plastic strips which could be independently aligned in the plane of the jet.

The clock consisted of a 115 volt AC synchronous speed motor to which was attached a metal hand. The motor speed was constant at 300 revolutions per minute. The clock face was marked with twenty divisions. Thus the clock hand passed a division in 0.01 second.

The jet was recorded by means of a 35 mm motion picture camera. The exposure time for each frame was 0.0015 second. The camera was run

at a speed of approximately 36 frames per second. The camera was positioned with the axis of the lens perpendicular to the plane of the jet. The camera was centered on the coordinate frame, and the lens was found to be free of excessive distortion by examination of photographs of the horizontal and vertical scales.

In order to obtain pressure measurements at different points along the pipe, piezometer holes were located at the downstream end of each pipe section. Four piezometer holes were drilled on orthogonal diameters with a No. 45 drill. These piezometer holes were located one-half inch upstream from the downstream end of each pipe section. The holes were rigidly inspected, and burrs caused by drilling were carefully scraped away with a sharp knife. A series of steady-flow tests was made with the pipe sections joined in order to check the geometric accuracy of both piezometers and pipe. The piezometric head gradients determined by these tests showed deviations not greater than one per cent from the Blasius smooth pipe data [14]. Individual pressure measurements at each piezometer resulted in deviations from the Blasius gradient no greater than 0.7 per cent of the total head, h_o.

The piezometer rings (Fig. 8) were cut in the pipe sleeve coupling and were completed by the brass transducer collar. Four holes were drilled in the pipe sleeve to coincide with the piezometer holes in the pipe section. The transducer collar was slipped over the pipe sleeve and was sealed in place by two brass pressure plates and two-inch "O" rings. Two holes were tapped in the collar, allowing

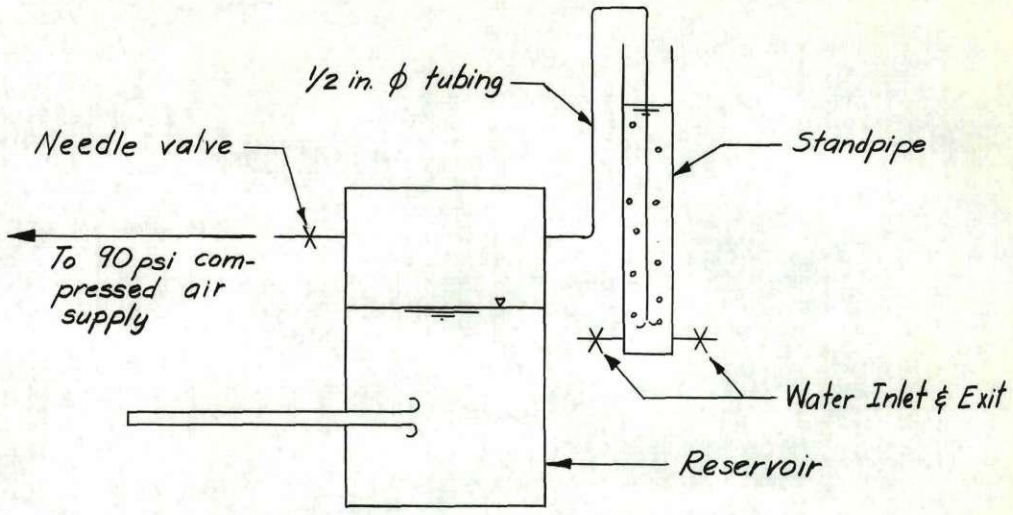

Fig. 7. Air pressure regulator

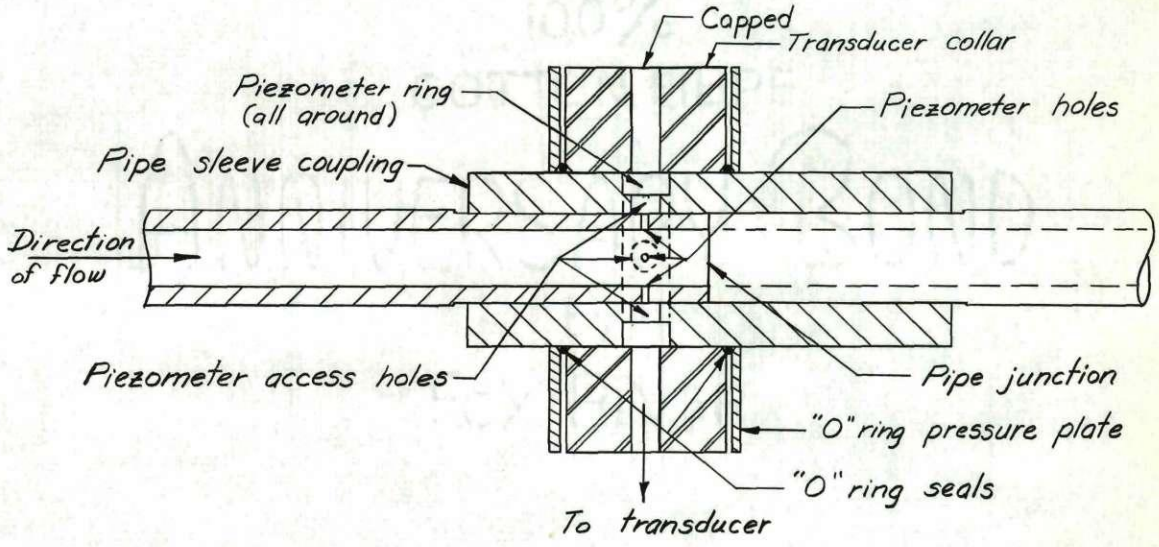

Fig. 8. Pipe sleeve coupling with piezometer ring

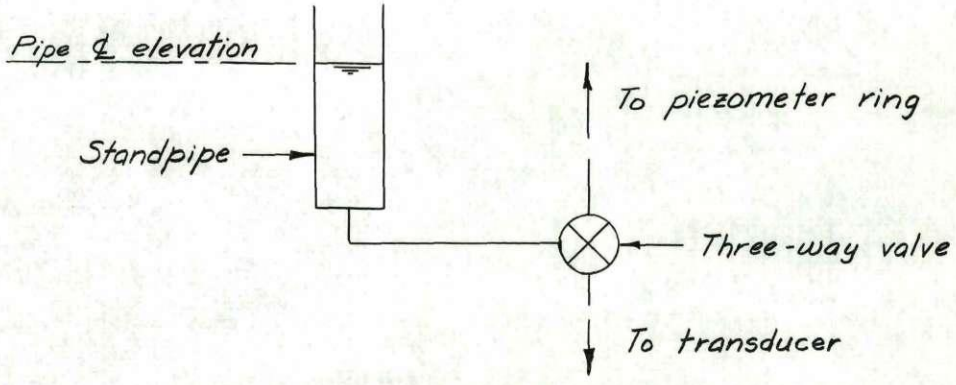

Fig. 9. Three-way valve arrangement

access to the piezometer ring. The upper hole was used to bleed all air from the ring and the lower was used to attach the pressure transducers.

The pressure measuring devices used were manufactured by Consolidated Engineering Corporation. The devices are known as Consolidated pressure transducers, Type 4-312, with a pressure differential range of ± 7.5 pounds per square inch. The transducers were connected to the collars by two methods. In the first method the transducer was directly attached to the collar by means of a pipe nipple (B, Fig. 6). In the second method a three-way valve was placed between the collar and the transducer (Fig. 9). A short standpipe was attached to one leg of the valve. The standpipe water surface elevation could be adjusted to the elevation of the pipe centerline, thus providing a reference base for the transducer deflections.

In order to measure pressure variations with time, a Sanborn Twin-Viso Cardiette Recorder, Model 60, was used to record the transducer impulses (H, Fig. 6). In the operation of this recorder an electrically heated stylus is deflected by a variable magnetic force in response to the electrical signal from the transducer. The heated stylus produces a continuous trace on sensitized paper from which the pressure variations can be determined. The sensitized paper is a continuous sheet which travels at a constant speed. Time measurements are obtained from "pips" produced by an independently actuated timing stylus on the sensitized paper.

Detailed description of technique.--In the preceding section a detailed physical description of the equipment was presented. In this section a

detailed description of the experimental techniques is presented.

Horizontal and vertical alignment of the pipe was attained to the nearest two thousandth of a foot. The pipe centerline elevation was established and transposed to the hook gage. The coordinate frame was placed parallel to the pipe and in such a position that the valve arm was very nearly vertical when in the closed position. Centering of the valve disk on the pipe outlet was accomplished by means of the leveling screws in the coordinate frame base. After the valve was centered, it was carefully closed so as to avoid any shearing force between the valve disk and the end of the pipe. It was observed that a shearing force at this junction could be responsible for undesirable pipe vibrations after the valve was released. Care had to be taken in closing the valve after each run in order to avoid water hammer pressures which could have overstressed the pressure transducers.

The coordinate grid scales were then aligned in the plane of the jet. A plumb bob was used to align the vertical scale so that it marked the end of the pipe.

The motion picture camera was centered on the coordinate frame with the lens axis perpendicular to the plane of the jet. After several trial runs, a small amount of red vegetable dye was introduced into the water and a red filter was attached to the camera lens. This practice resulted in a very clear picture of the jet. The dye concentration was on the order of 0.03 of one per cent by volume. The assumption was made that this low concentration would not change the properties of water.

The pressure transducers were placed at the desired position on the pipe and the piezometer rings were bled of all air which might have become entrapped in the pipe. The reservoir was allowed to settle at least four or five hours after each disturbance before any runs were attempted. Excessive line voltage variations during the day affected the pressure transducer records and necessitated that runs be taken at night or very early in the morning. The practice generally followed was to make one run per night.

Immediately prior to running a test, the temperature of the water was recorded. Utilizing this temperature the required head of water was computed in order to obtain the desired value of the head parameter. The manometer was then referenced to the pipe centerline from the properly adjusted water level in the hook-gage well. Knowing the required head and therefore the required manometer deflection, the desired manometer reading was then calculated. This manometer reading was used to indicate the correct head in the reservoir.

To produce the desired effective head, air from a compressed-air source was admitted into the sealed reservoir above the water. By adjustment of the water level in the standpipe, the air pressure in the reservoir could be controlled. The operation of the water standpipe air pressure regulator was not as expected, but proved to be very satisfactory. The expected operation (Fig. 7) was based on the premise that as long as air bubbled from the submerged end of the tubing, the pressure of the air throughout was equivalent to the height of water in the standpipe. This proved to be erroneous due to the head losses in

the tubing. Therefore, the air pressure in the reservoir was a function of both the water height in the standpipe and the flow of air through the system. The flow of air was further complicated by the fact that the supply air pressure was not a constant. The varying supply air pressure produced a continually changing flow which, although not rapid, necessitated continuous observation and adjustment in the needle valve control. The flat nature of the piezometric grade line in the tubing was deemed an advantage, for the reservoir air pressure could be minutely controlled by varying the rate of air flowing through the system. The procedure followed was to record the final manometer reading immediately before instigating each run.

The water level in the reservoir was kept at approximately twenty inches above the pipe centerline. This depth was chosen in consideration of both the effect of restricting the flow into the rounded pipe inlet and the drawdown effect on the air pressure during flow establishment. No make-up water was added during flow establishment. The reservoir diameter proved to be large enough to prevent excessive drawdown.

The accuracy of each computed head parameter $gh_oD^3/L\upsilon^2$ (Table I, APPENDIX) is on the order of $\pm$ 0.4 per cent. The desired head parameter value, that is, 30×10^6, 18×10^6, or 6×10^6, and so forth, was attained within an accuracy of $\pm$ 1.0 per cent.

Pressure measurements at different points along the pipe were obtained by the use of two pressure transducers and an oscillograph recorder. Two procedures were followed in this operation.

Initially the transducers were calibrated and their calibration curves were applied to the recorded deflections. The transducers were

balanced on the total head and deflections were measured from that base-line. The drawback to this method was the dependence upon the accuracy of the calibration curves.

Finally, by means of a three-way valve arrangement (Fig. 9), the use of the transducers was refined to eliminate all calibration curves. The transducers were first balanced using the pipe centerline reference base. The three-way valve was switched so as to allow the transducer to receive the pressure in the pipe. The oscillograph was adjusted to allow the maximum deflection of the recording stylus. Thus was recorded a deflection for each measured head, and subsequent deflections could be compared with the initial deflection.

The downstream valve arrangement, as has been explained in the previous section, required rapid release of the secondary spring. This rapid release was obtained by two methods. The first method required the release of the secondary spring by quickly disengaging a hook arrangement. The hook was attached to the end of the secondary spring and was hooked over a small pin located in the rotating arm (D, Fig. 6). This releasing procedure, although producing a satisfactory valve action, was deemed too susceptible to variations in operator technique and was replaced by a second method. This second method consisted of a horizontal secondary spring (in place, but unextended at D, Fig. 6) which was extended and secured by a single wire strand to the valve arm. Sharp wire cutters were then used to cut the wire strand and release the secondary spring.

During a run the procedure followed was to balance the transducers, start the oscillograph recording mechanism, read the manometer,

allow the camera to attain its operating speed, and quickly open the valve. The run was completed when the jet became turbulent and steady.

CHAPTER IV

EXPERIMENTAL RESULTS

In the preceding chapter a detailed description of the experimental equipment and experimental technique was presented. In this chapter a detailed statement of the results of this study is presented.

Determination of velocity.—The direct experimental data consisted of a series of motion picture film strips of the jet which issued from the pipe. Two assumptions were utilized in order to determine velocity from the photographically recorded jet. First, air resistance was negligible. Second, the jet was considered to be a succession of fluid masses comprised of individual fluid particles each having the velocity characteristics of this larger group. If the velocity characteristics of the individual particles of a fluid mass are identical, the motion can be completely described by the motion of the mass center of that fluid mass.

Utilizing the two preceding assumptions, a jet discharging freely into the atmosphere is acted on by the acceleration of gravity alone. Figure 10 is a schematic sketch of the jet trajectory of such a jet. The initial horizontal component of the velocity must necessarily remain the same throughout the free fall. If the pipe is horizontal, then the horizontal velocity component of the particle will represent the fluid velocity when the particle was at the outlet.

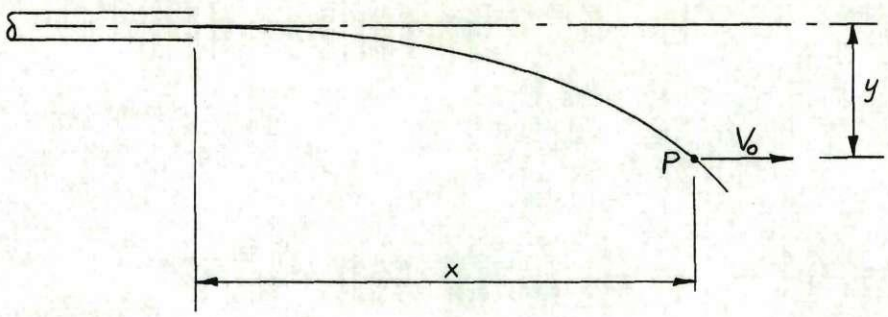

Fig. 10. Jet trajectory

From a free falling body with no resistances,

$$y = \frac{gt'^2}{2} \tag{26}$$

where g is the acceleration of gravity, t' is the time elapsed since the particle left the pipe outlet, and y is the vertical distance the particle has fallen. From Eq. (26)

$$t' = \sqrt{\frac{y}{g/2}} \tag{27}$$

Again assuming no resistances,

$$x = V_o t' \tag{28}$$

where V_o is the horizontal component of the velocity of the particle at any point in the jet and x is the horizontal distance traveled in time t'. Thus by using Eqs. (27) and (28) with the jet coordinates of the freely falling particle, one can obtain the initial horizontal velocity and also the time which has elapsed since the particle left the pipe outlet. If there is an arbitrary time T at which the particle P is at

the position (x, y), then the arbitrary time at which the particle P with velocity V_o was at the pipe outlet is T minus t'.

The 35-mm film strip was used to obtain the velocity-time relationship. The timing clock is pictured in all frames of the film strip. Hence the time interval T between the film strip frame and the valve opening could be determined from the clock reading as recorded on that frame.

In order to accurately measure the observed velocities V', each film strip was projected onto a screen marked with a grid system. The projector was adjusted to align the image vertically and horizontally on the grid and to insure the absence of scale distortions. The coordinate measurements were then taken from the projected image. The horizontal and vertical distances were measured from the end of the pipe and the pipe centerline respectively. The time t' of vertical fall was calculated from the vertical measurement by means of Eq. (27). With this time and the measured horizontal distance x, the observed velocity of the fluid when leaving the pipe was computed by means of Eq. (28). The frame time T was recorded for each particle so measured. This frame time minus the time of particle fall is the time interval t from the time of valve opening to the time at which the measured particle was at the pipe outlet.

Figure 11 is a series of frames selected from the film of Run 29. The frames were selected to illustrate the sequence of events in jet development. The times given are frame times T. Figure 11 (a) is an illustration of a good valve opening. The first particle of laminar flow fell almost straight down, approaching an observed velocity of zero. The peculiar curvature of the laminar jet in Fig. 11 (b) and (c) is explained

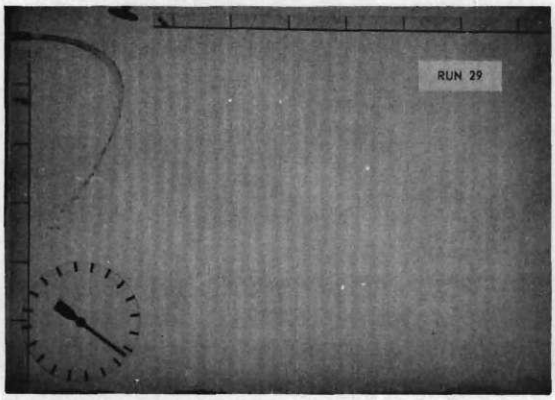

(a) T = 0.355 SEC.

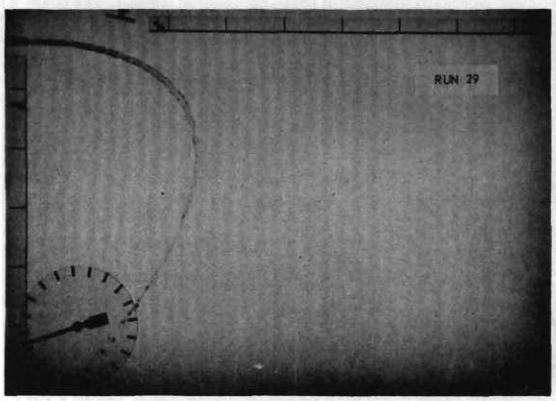

(b) T = 0.466 SEC.

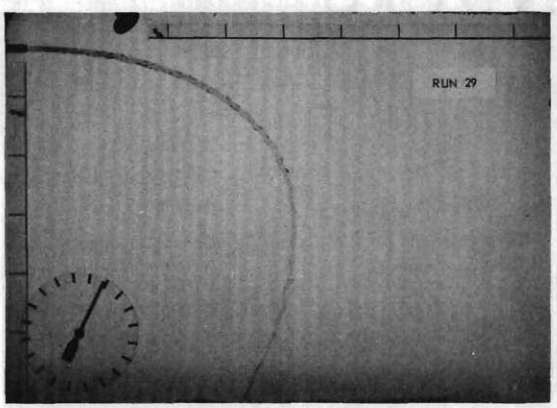

(c) T = 0.511 SEC.

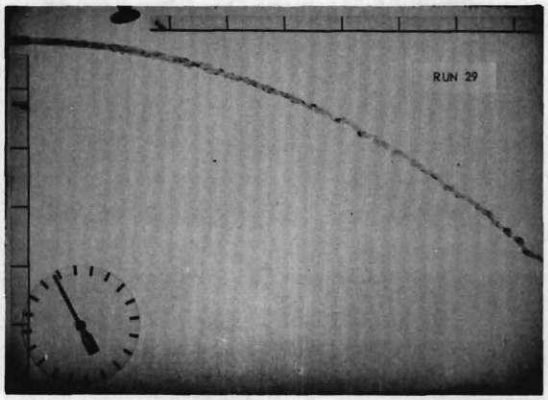

(d) T = 1.222 SEC.

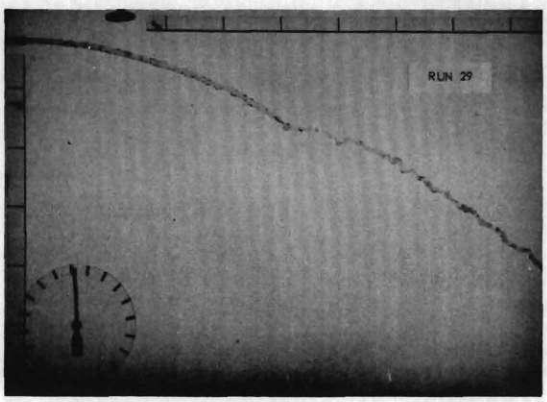

(e) T = 1.607 SEC.

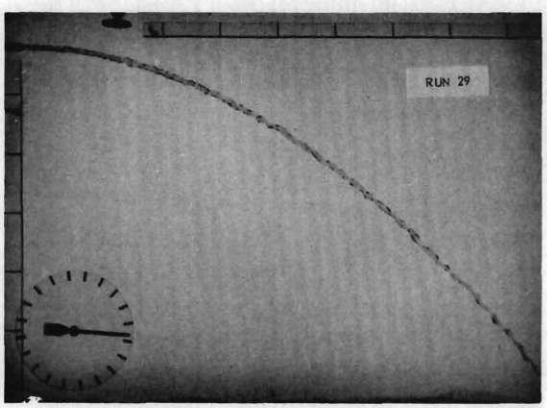

(f) T = 1.953 SEC.

Figure 11. Sequence of events in jet development.

by noting that these are streak lines as differentiated from path lines. On Fig. 11 (d) is shown laminar flow approaching the steady state. Figure 11 (e) is an illustration of the abrupt transition from laminar to turbulent flow. Fluid on the right is in the laminar state while that on the left is in the turbulent state. The steady turbulent state is shown on Fig. 11 (f). This trajectory represents both a streak line and a path line since the flow is steady.

It is apparent from Fig. 11 that an infinite number of observed velocities may be obtained from each film strip. The technique generally followed was to evaluate only the one point of each frame at a y of 2.50 feet. At the transition between laminar and turbulent flow many points were evaluated to insure proper definition of the transition.

On Figs. 12 through 16 are presented the observed velocity-time relationships as determined in the manner outlined above. As a check on the accuracy of this method of determining velocity, a steady flow test was made. The weight-time determination of the discharge was made both before and after photographing the steady flow jet. The velocities determined by means of the jet photographs were 1% greater than by means of the weight-time measurement. The higher value determined from the photographs was an indication that the air resistance on the jet is negligible.

An additional check of the assumption of negligible air resistance was made by determining the observed velocity of the same particle at different values of the vertical distance y. If air resistance were negligible, the observed velocity would be constant irrespective of the value of y. These observed velocities were practically identical whether

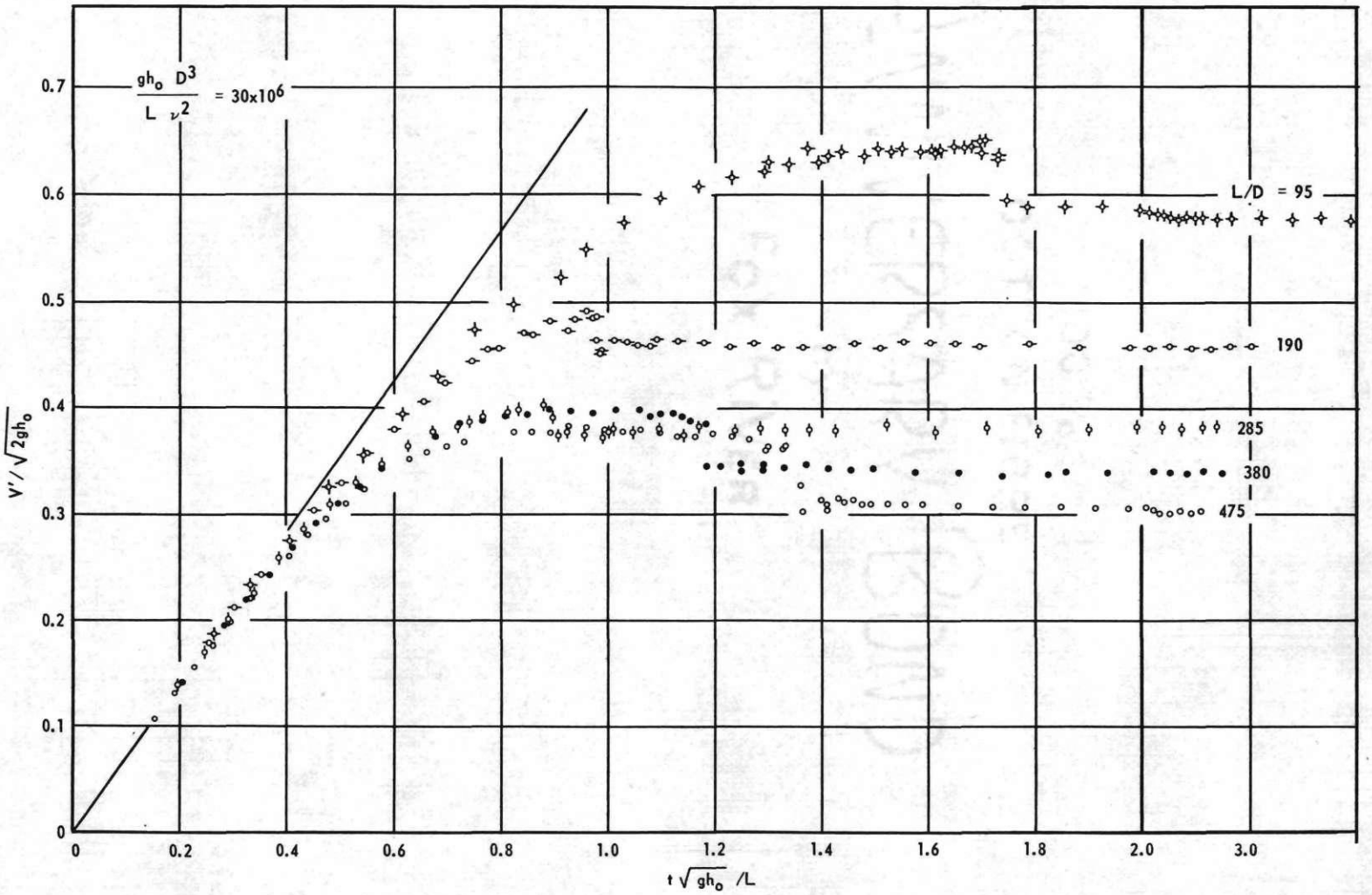

Figure 12. Observed velocity-time data with $gh_oD^3/L\nu^2 = 30 \times 10^6$.

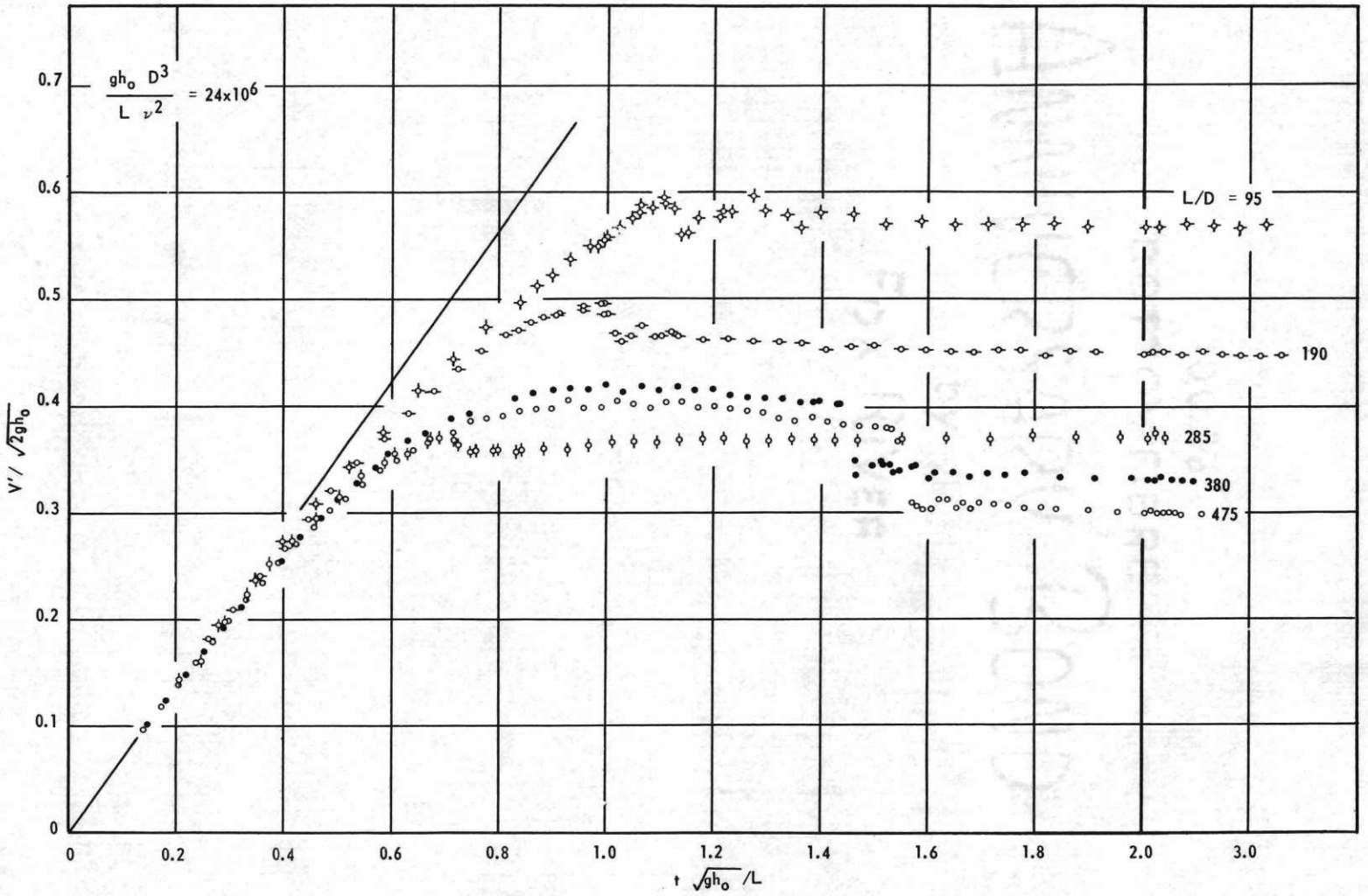

Figure 13. Observed velocity-time data with $gh_oD^3/L\nu^2 = 24 \times 10^6$.

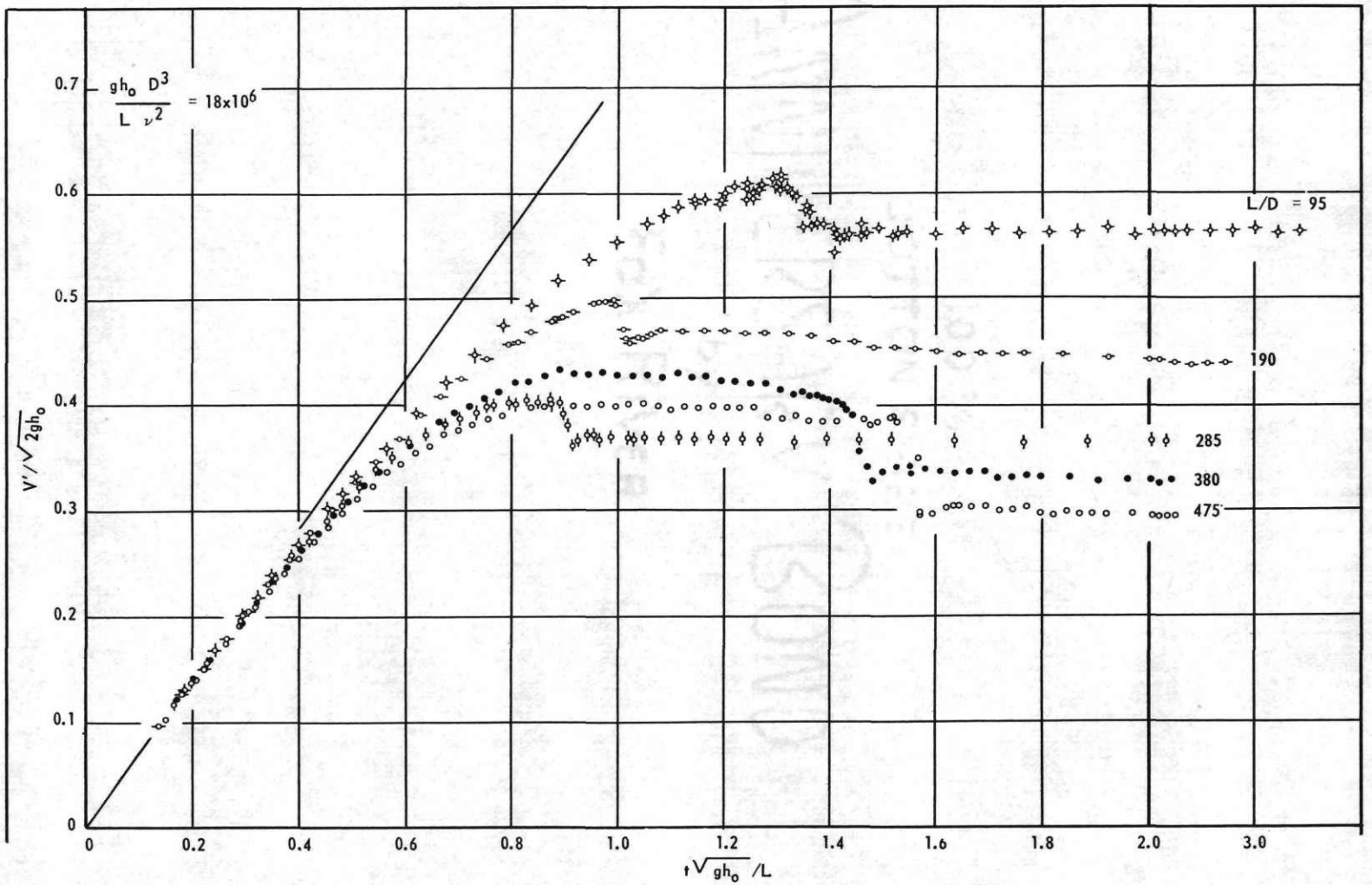

Figure 14. Observed velocity-time data with $gh_oD^3/L\nu^2 = 18 \times 10^6$.

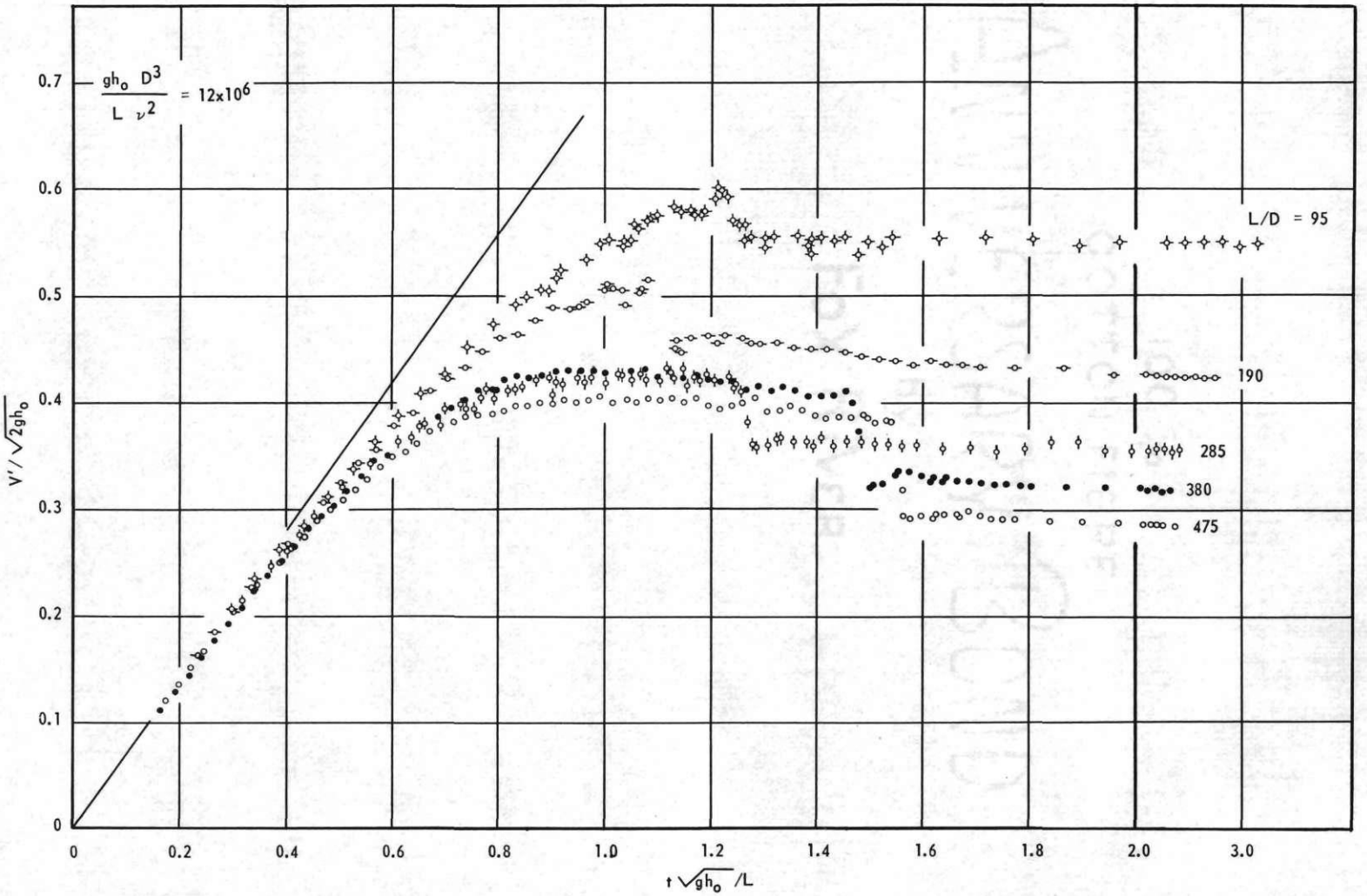

Figure 15. Observed velocity-time data with $gh_oD^3/L\nu^2 = 12 \times 10^6$.

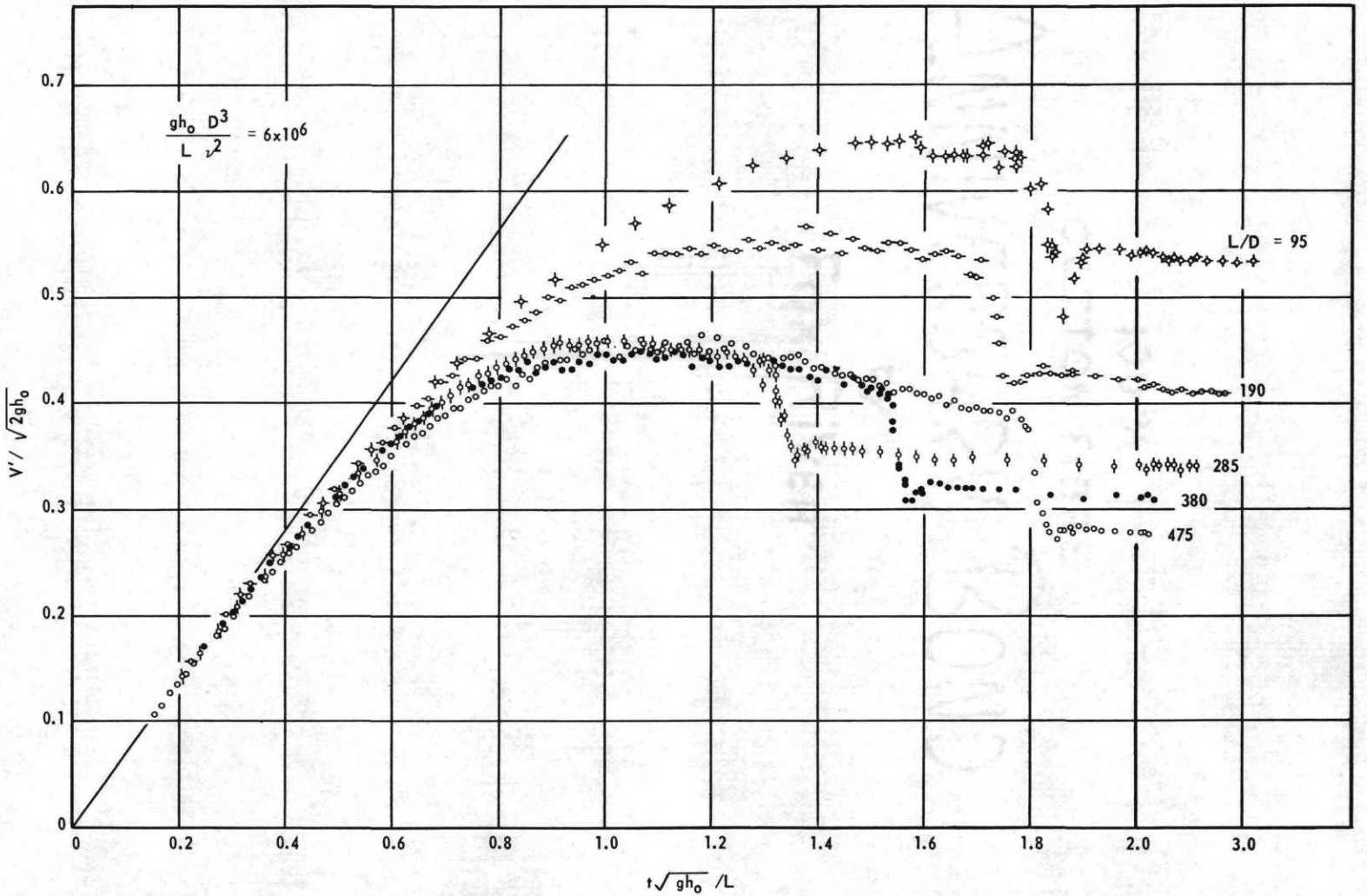

Figure 16. Observed velocity-time data with $gh_oD^3/L\nu^2 = 6 \times 10^6$.

computed at a vertical distance y of 2.50 feet or 0.50 foot. On the basis of these results, the assumption of negligible air resistance is valid.

The assumption that the jet can be visualized as a series of individual fluid masses is apparently borne out by the formation of slugs of fluid in the jet. Figure 11 shows this phenomenon to a marked degree. In order for the jet to be considered as a series of individual masses, a lateral transfer of linear momentum must take place. As the jet leaves the pipe, there exists a radial variation of linear momentum across the jet as a result of the radial variation of the velocity. This radial variation of the velocity is caused by internal shearing stresses which originate at the pipe wall. The internal shear stress is directly proportional to the velocity gradient. Once the jet leaves the pipe outlet, the external shearing force, at the pipe wall is removed from the elemental slug of the jet. There still exists, however, a velocity gradient which results in internal shear stresses. These internal shear stresses are now the implement by which the momentum transfer takes place. The shear stresses act to retard the particles with an excess in linear momentum and accelerate those particles with a lesser amount of linear momentum. Thus the elemental slug of the jet will become a mass of fluid in which all of the particles can be represented by the mass center. The same check used for proof of the assumption of negligible air resistance is now used to check the transfer of linear momentum. Since the observed velocities did not vary with vertical distance y of 2.50 feet or 0.50 foot, the linear momentum transfer apparently is quite rapid, and is completed before reaching the vertical distance y of 0.50

foot. Incomplete momentum transfer with jet separation is discussed in detail in a later section. A detailed discussion of the effect of velocity distribution on the relationship between mean velocity V and observed velocity V' is given in the following section.

Corrections of observed velocity-time curves.--A non-uniform velocity distribution in the jet at the pipe outlet will have an effect on the geometry of the jet downstream from the outlet. The relationship between the observed velocity of the jet and the mean velocity in the pipe can readily be evaluated from the principles of conservation of momentum. The assumptions which were previously made are (1) that at the point of measurement all fluid particles have the same velocity, (2) that the only external force on the jet is gravity, and (3) that the pipe is horizontal at the outlet. The mass of fluid under consideration is $\rho \forall$ in which $\forall$ is the volume of the fluid segment being considered. The linear momentum in the horizontal direction of this mass at the point of measurement is $\rho \forall V'$. The mass of fluid constituting this segment was ejected at the pipe outlet in an interval of time Δt. Thus

$$\rho \forall = \rho VA \, \Delta t = \rho \, \Delta t \int^{A} v \, dA \qquad (29)$$

in which A is the total cross sectional area of the pipe outlet, V is the mean velocity of flow at the pipe outlet, and v is the point velocity of the differential area dA. Since no horizontal external forces act on the jet, the horizontal linear momentum is constant. Hence

$$\rho \forall V' = \rho \, \Delta t \int^{A} (v)^2 \, dA \qquad (30)$$

Multiplying and dividing the right side of Eq. (30) by V^2 and employing Eq. (29), Eq. (30) reduces to

$$V' = \frac{V}{A} \int^{A} \frac{(v)^2}{(V)^2} \, dA \tag{31}$$

But

$$\frac{1}{A} \int^{A} \frac{(v)^2}{(V)^2} \, dA = K_m \tag{32}$$

where K_m is the momentum correction factor. Substituting Eq. (32) in Eq. (31) and rearranging results in

$$V = V'/K_m \tag{33}$$

or

$$V/\sqrt{2gh_o} = \frac{V'/\sqrt{2gh_o}}{K_m}$$

Thus it is imperative that the velocity distribution at the pipe outlet be known. Correction of the observed velocities $V'/\sqrt{2gh_o}$ to give the mean velocities $V/\sqrt{2gh_o}$ would otherwise be impossible.

The problem of velocity distribution in a pipe has been extensively studied for steady flow conditions, both laminar and turbulent. Prandtl [14] has developed an expression for the turbulent velocity distribution using the Blasius resistance law [14] for turbulent flow in smooth pipes as found by experiment. The expression is known as the seventh-root law of turbulent velocity distribution

$$\frac{v}{v_{max}} = \left[\frac{y}{r_o}\right]^{1/7} \tag{34}$$

in which y is the distance from the pipe wall, r_o is the radius of the pipe, v is the point velocity at y, and v_{max} is the maximum point velocity. With the velocity distribution of Eq. (34), K_m has the value of 1.02 and K_e has the value of 1.06. This expression is valid for steady turbulent flow in smooth pipes with Reynolds numbers below 100,000. The assumption is made that the values of K_m and K_e have the same value for unsteady turbulent flow in smooth pipes as for steady flow. The maximum Reynolds number attained in this experimental study was 50,800.

The assumption of the velocity distribution in laminar flow has been previously stated in Chapter II. The value of K_m is presented in Eq. (23) as a function of the relative boundary layer thickness n. Due to the complexities of determining n from a purely theoretical standpoint, the writer will now present three methods of determining n using empirical results.

Method I is the most accurate method for obtaining n since in this method the temporal and spatial variation of n does not affect the result. But, with this method only one value of n can be determined per run. The observed velocity-time curves of Figs. 12 through 16 inclusive are used for this method and are represented by Fig. 17 below.

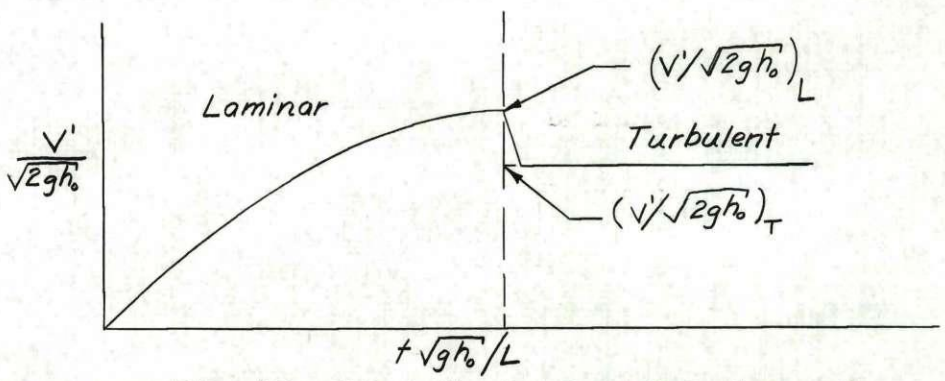

Fig. 17. Schematic drawing of an observed velocity-time curve.

The basis for this method is the fact that at the transition between laminar and turbulent flow, the mean velocity is essentially constant. The time of the transition is approximately at the first abrupt break in the laminar portion of the curve. This is based on results of the pressure-time study.[1] Therefore, by extrapolating the turbulent portion of the curve back to the time of transition, the different values of $V'/\sqrt{2gh_o'}$ may be obtained. Since K_m for turbulent flow is assumed a constant 1.02, then, at the time of the transition,

$$(K_m)_L = 1.02 \frac{(V'/\sqrt{2gh_o'})_L}{(V'/\sqrt{2gh_o'})_T} \tag{35}$$

Since $(K_m)_L$ is a function of n, the value of n may be indirectly determined. The results of Method I are presented in Table III of the APPENDIX.

Method II employs both the observed velocity curves shown in Figs. 12 through 16 and the pressure data of this study. This method employs the sharp rise in pressure recorded when the interface between laminar and turbulent flow passes a piezometer (Fig. 18). As the flow progresses in the pipe, the transition from laminar to turbulent flow passes a piezometer at a time $t\sqrt{gh_o'}/L$. At that time a sharp pressure rise is noted on the pressure-time curve. Since the total energy level at this instant is essentially constant to the left and to the right of the laminar-turbulent interface, the difference in pressure must be due to the difference in kinetic energies of the two flow regimes. K_e for

---

[1] The pressure data of this study is presented in Parts II and III.

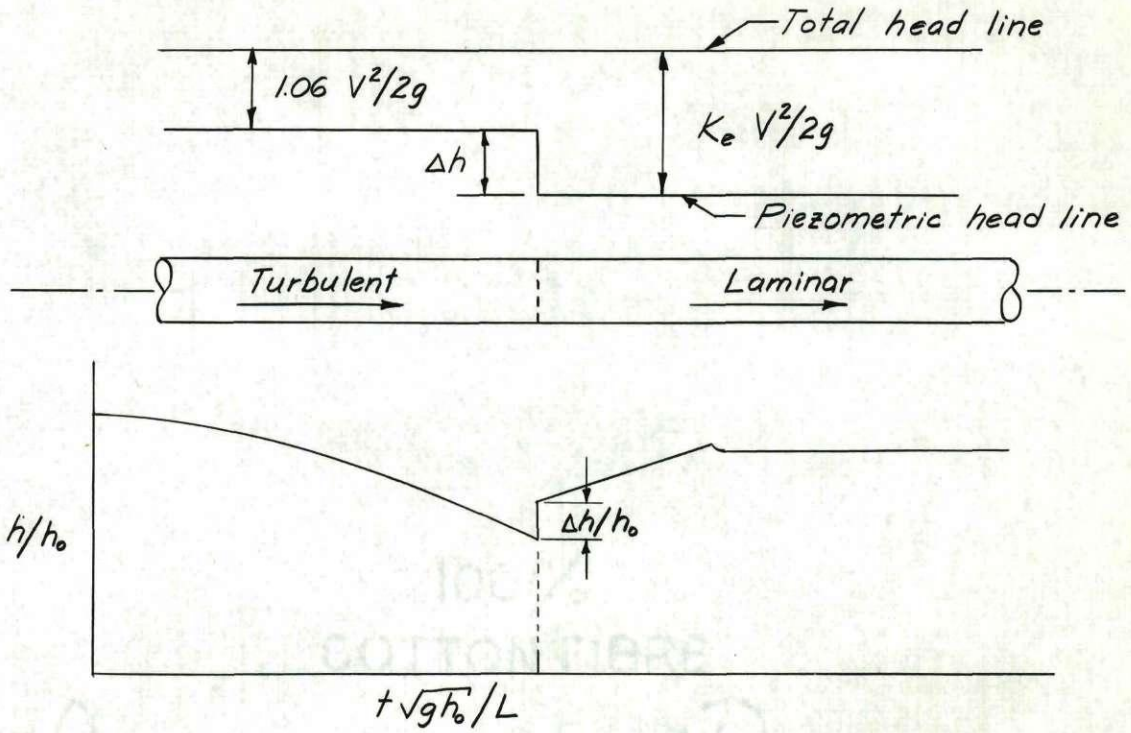

Fig. 18. Schematic diagram of transitional pressure change.

turbulent flow is assumed constant at 1.06. Therefore

$$\Delta h = K_e \frac{V^2}{2g} - 1.06 \frac{V^2}{2g} = \frac{V^2}{2g} (K_e - 1.06) \tag{36}$$

where Δh is the change in piezometric head. Dividing Eq. (36) by h_o and utilizing Eq. (33) leaves

$$\frac{\Delta h}{h_o} = \frac{(V'/\sqrt{2gh_o})^2}{(K_m)^2} (K_e - 1.06) \tag{37}$$

Since K_m and K_e are both functions of n, the assumption is made that the boundary layer thickness is the same at the pipe outlet as at the point of pressure measurement. This assumption is necessary to allow the following step to be taken. Thus

$$\frac{\Delta h/h_o}{V'/\sqrt{2gh_o}} = \frac{K_e - 1.06}{K_m^2} \tag{38}$$

The right side of Eq. (38) is a function of n alone. The left side may be determined from the experimental data. Thus the value of n was determined for the time at which the transition passed a piezometer. The results of Method II are presented in Table III of the APPENDIX.

Method III for the determination of an empirical n, like Method II, employs both the observed velocity data and the pressure data. The linear momentum equation, Eq. (25), developed in Chapter I is the basis for this method. Dividing Eq. (25) by $\gamma h_o/D$ gives

$$-\frac{\partial(h/h_o)}{\partial(x/D)} - \left[\frac{16\,\upsilon\,V}{gh_o\,D}\right]\left[\frac{1}{n}\right]\left[\frac{6}{6-4n+n^2}\right] = \frac{D}{gh_o}\,\frac{dV}{dt} \tag{39}$$

where γ is the unit weight of the fluid. But

$$\frac{dV}{dt} = \frac{\sqrt{2}\,gh_o}{L}\,\frac{d(V/\sqrt{2gh_o})}{d(t\,\sqrt{gh_o}/L)}$$

and

$$\frac{16\,\upsilon\,V}{gh_oD} = \frac{16\sqrt{2}\;\;V'/\sqrt{2gh_o}}{\sqrt{(L/D)(gh_oD^3/L\upsilon^2)}\;K_m}$$

Substitution of the above terms in Eq. (39) and rearranging gives

$$\left[\frac{1}{K_m}\right]\left[\frac{1}{n}\right]\left[\frac{6}{6-4n+n^2}\right] = \frac{\sqrt{(L/D)(gh_oD^3/L\upsilon^2)}}{16\sqrt{2}\;\;V'/\sqrt{2gh_o}}\left[-\frac{\partial(h/h_o)}{\partial(x/D)} - \frac{2}{L/D}\,\frac{d(V/\sqrt{2gh_o})}{d(t\sqrt{gh_o}/L)}\right] \tag{40}$$

The left side of Eq. (40) is a function of n alone. The right side can be determined from experimental data. Within the brackets on the right side of Eq. (40) is, first, the slope of the dimensionless piezometric grade line and, second, a term containing the dimensionless acceleration $\frac{d(V/\sqrt{2gh_o})}{d(t\sqrt{gh_o}/L)}$ of the mean velocity-time curves. Inasmuch as the value of the dimensionless acceleration is a function of the corrected value of $V/\sqrt{2gh_o}$, the solution necessarily was one of successive approximation. Using the results from Method I and II, a very good first approximation could be made for the function of n with time. The corrected or mean velocity curves, obtained from the assumed n-t curves, were plotted and the dimensionless accelerations were determined. The piezometric head lines were plotted at fixed levels of time, that is, $t\sqrt{gh_o}/L = 0.2$, 0.4, and so forth. The piezometric head gradient was determined from these working graphs in the region where the gradient was constant. The corresponding $V'/\sqrt{2gh_o}$ and $\frac{d(V/\sqrt{2gh_o})}{d(t\sqrt{gh_o}/L)}$ were obtained and substituted in Eq. (40). Thus, with the other constants of the run, the function of n could be computed, which indirectly gave a value of n. Repeating this procedure for various values of $t\sqrt{gh_o}/L$ defined the empirical relationship of the n-t function. This empirical relationship was compared with the assumed relation and adjustments were made where necessary. The results of Method III are presented in Table III of the APPENDIX.

The final mean velocity-time curves are shown on Figs. 19 through 23. The final mean velocity-time curves are believed to be within ± 4 per cent of the true values. These curves are plotted at a constant level

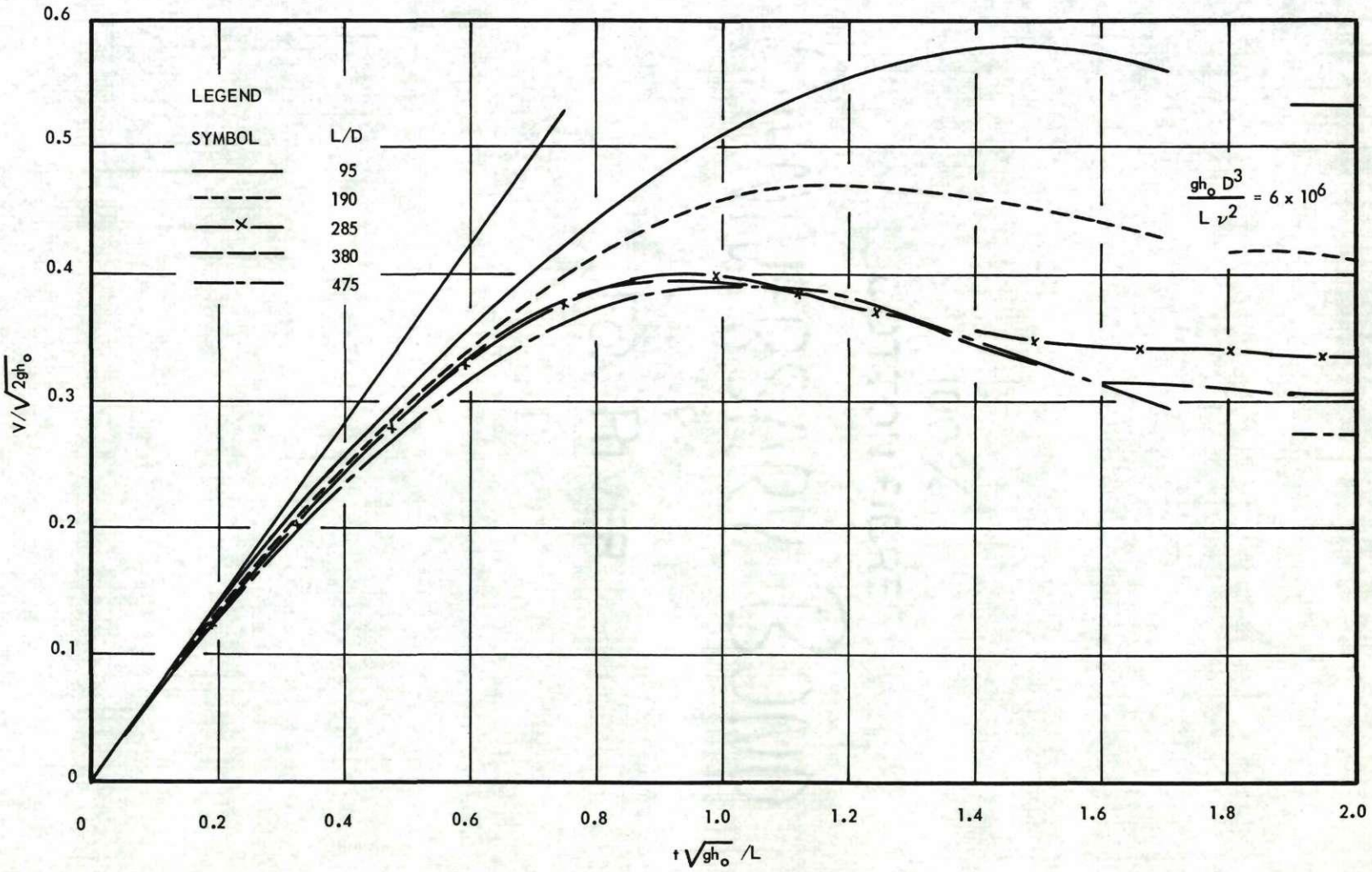

Figure 19. Mean velocity-time curves with $gh_oD^3/L\nu^2 = 6 \times 10^6$.

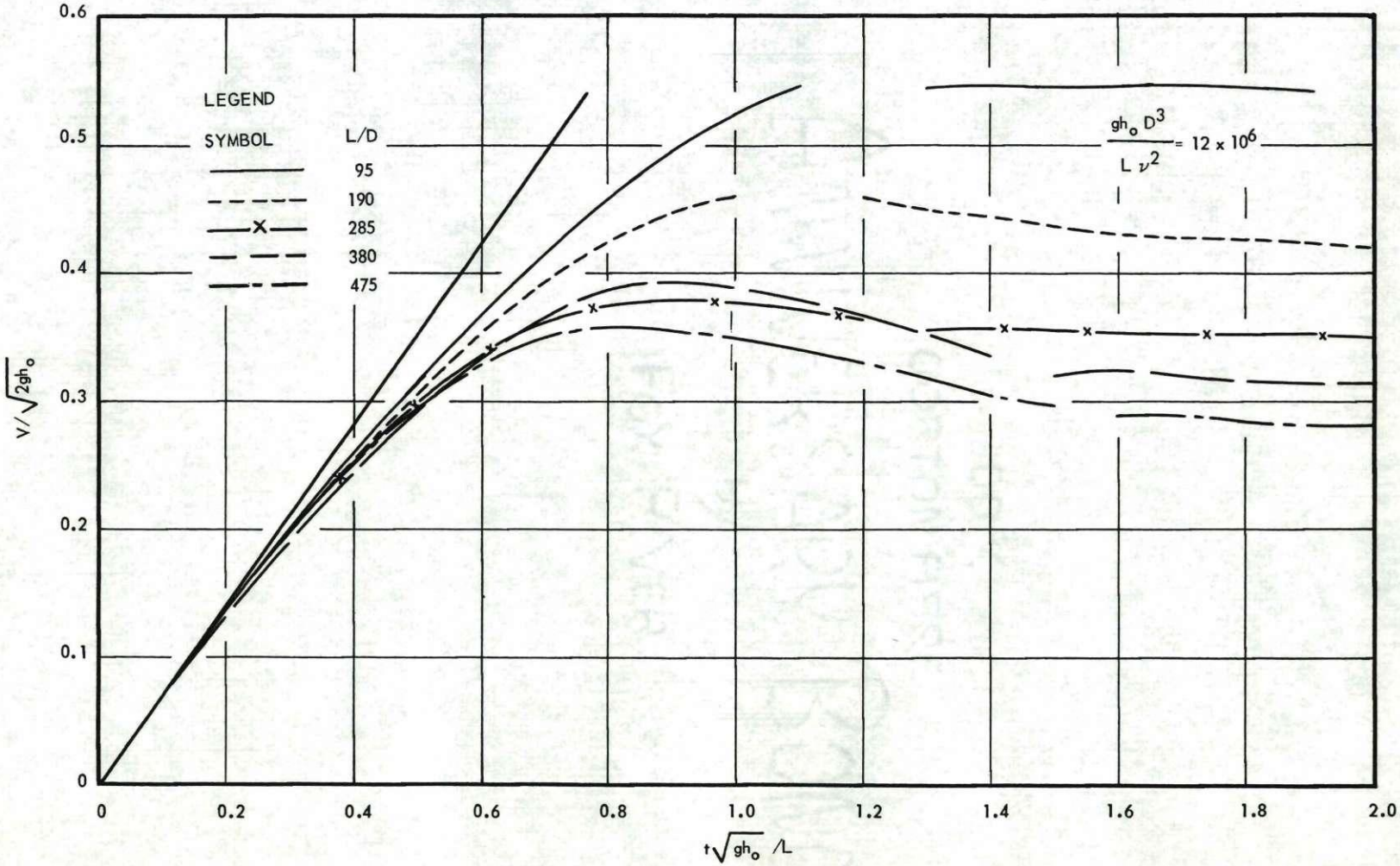

Figure 20. Mean velocity-time curves with $gh_oD^3/L\nu^2 = 12 \times 10^6$.

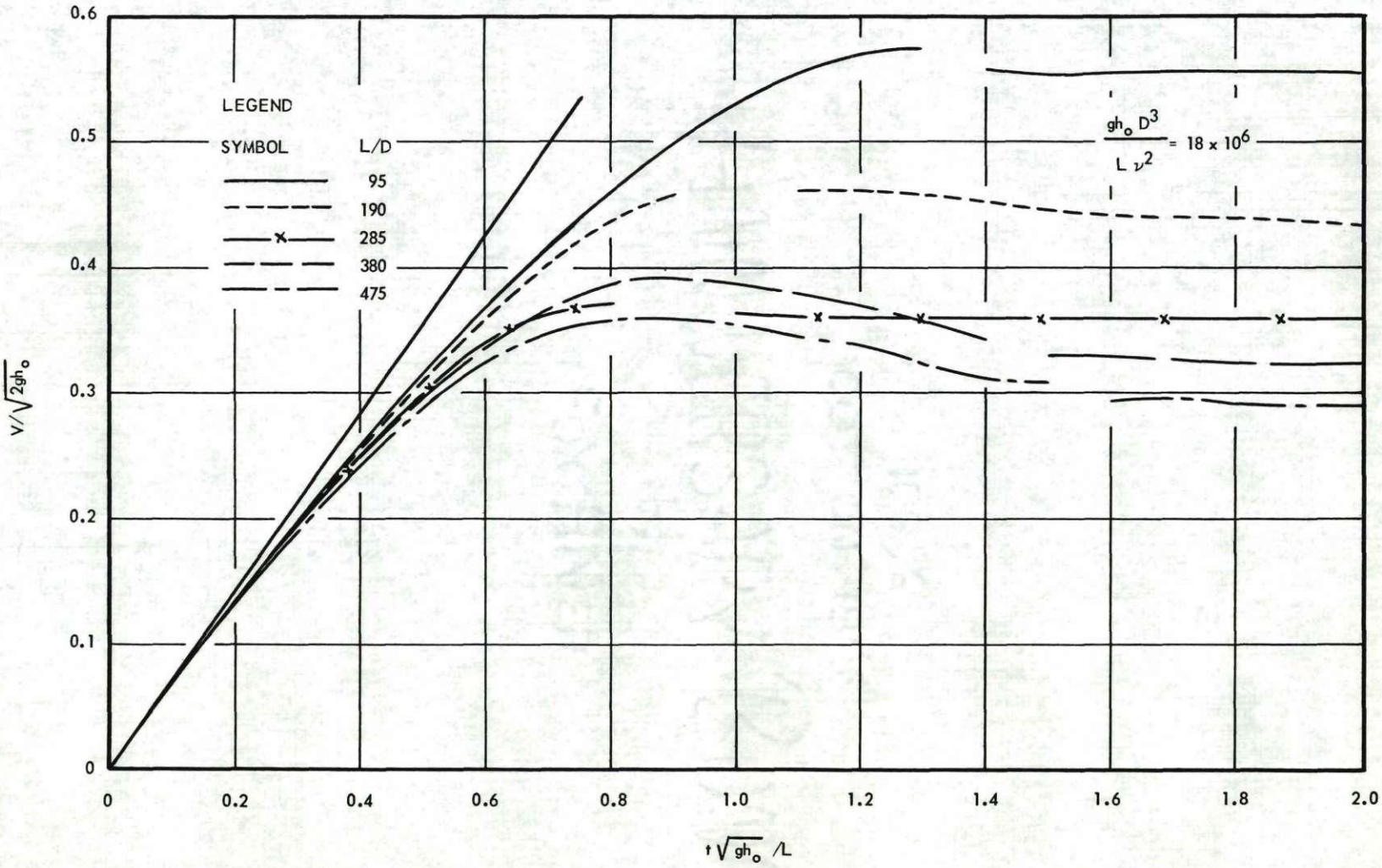

Figure 21. Mean velocity-time curves with $gh_oD^3/L\nu^2 = 18 \times 10^6$.

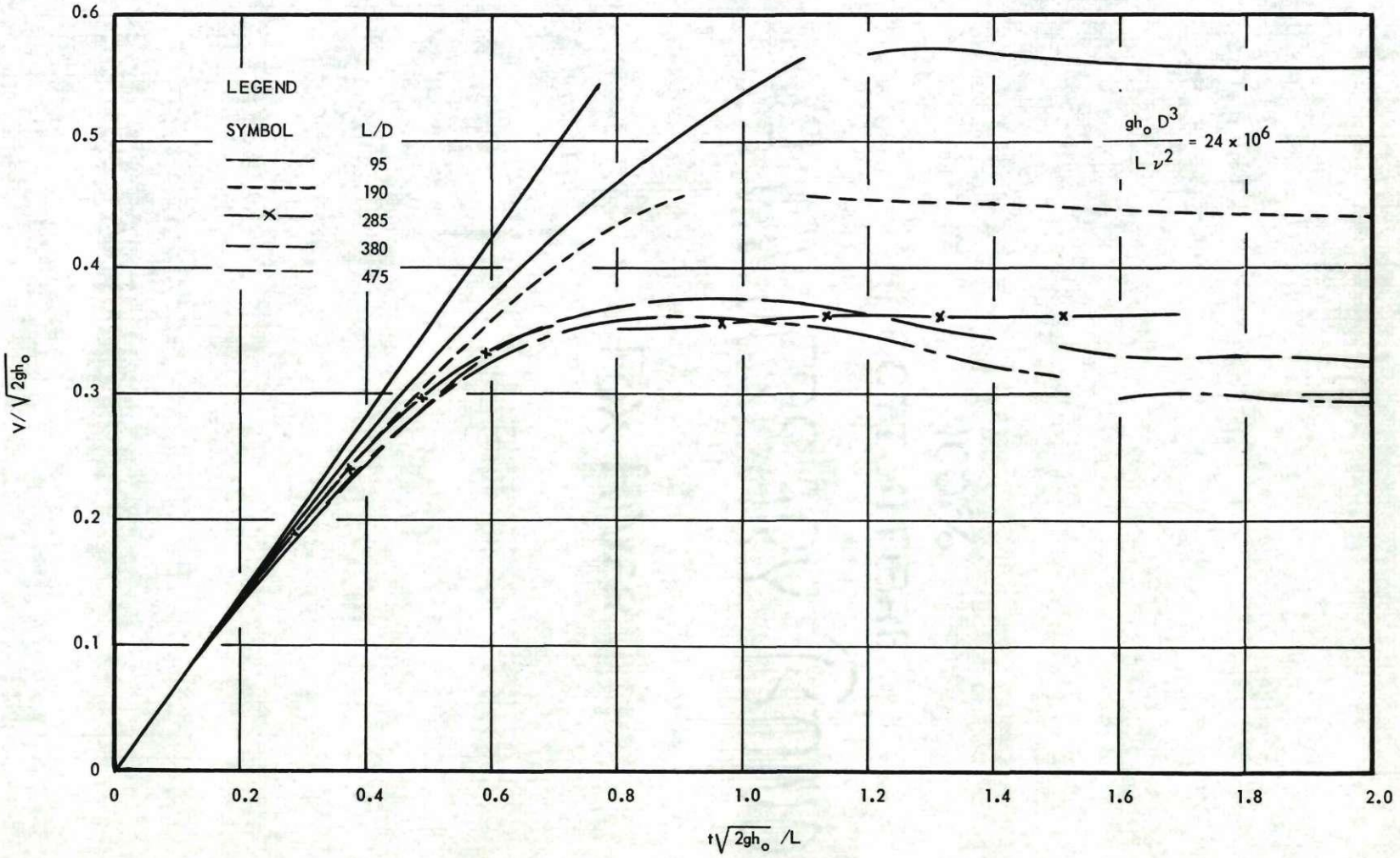

Figure 22. Mean velocity-time curves with $gh_oD^3/L\nu^2 = 24 \times 10^6$.

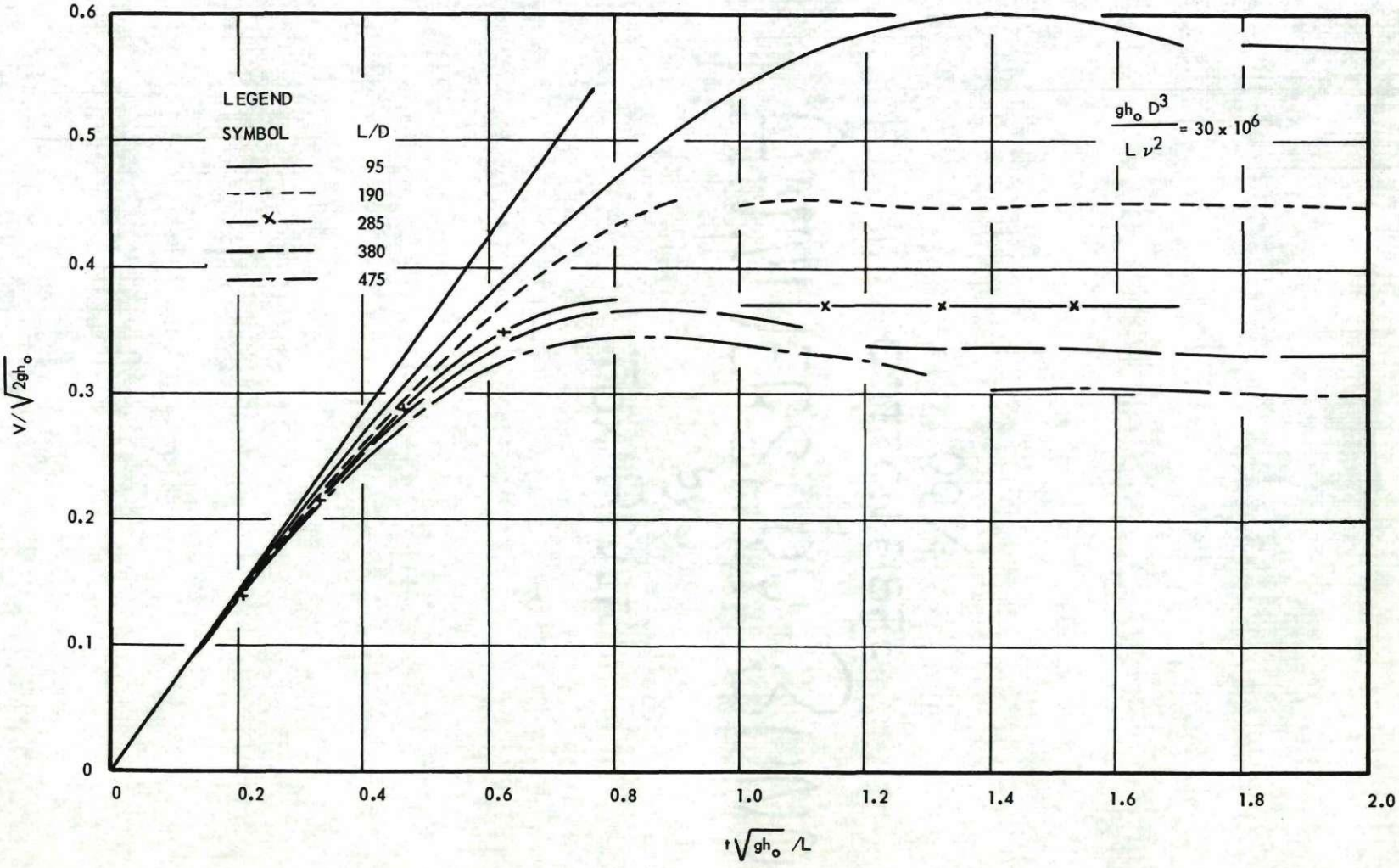

Figure 23. Mean velocity-time curves with $gh_oD^3/L\nu^2 = 30 \times 10^6$.

of the head parameter $gh_o D^3/L\upsilon^2$. Thus the effects of variation in the length parameter L/D is readily seen. Figures 24 through 28 are also the final mean velocity-time curves. These curves are plotted at constant values of L/D. Thus the effect of variation in $gh_o D^3/L\upsilon^2$ is illustrated.

Jet separation.--The jet downstream from the pipe outlet separated in characteristic laminar fashion during the flow establishment of four runs. These runs were Runs 20, 25, 26, and 27. The values of the time parameter at which separation first occurred are respectively 1.00, 0.80, 1.00, and 1.32. The jet separated in such a manner (Fig. 29) that the inner core remained together and the outer portion was progressively shed from the inner. This jet separation is the result of incomplete linear momentum transfer. The transfer of linear momentum has been previously explained. Pronounced variation in the velocity distribution would necessarily cause a greater relative value of shear stress within the jet. However, this pronounced variation would also represent a still greater relative variation in the linear momentum across the jet. Thus a condition is reached in which the internal shear force is no longer capable of causing the equalization of linear momentum across the flow. Then the jet separates. Since the velocity distribution of the jet can result in jet separation, it appears that there will be a jet separation limit to the non-uniformity of velocity distribution. This limit was found to be a value of n of 0.65 from the results of Method I. Jet separation did not occur for any value of n equal to or less than 0.65.

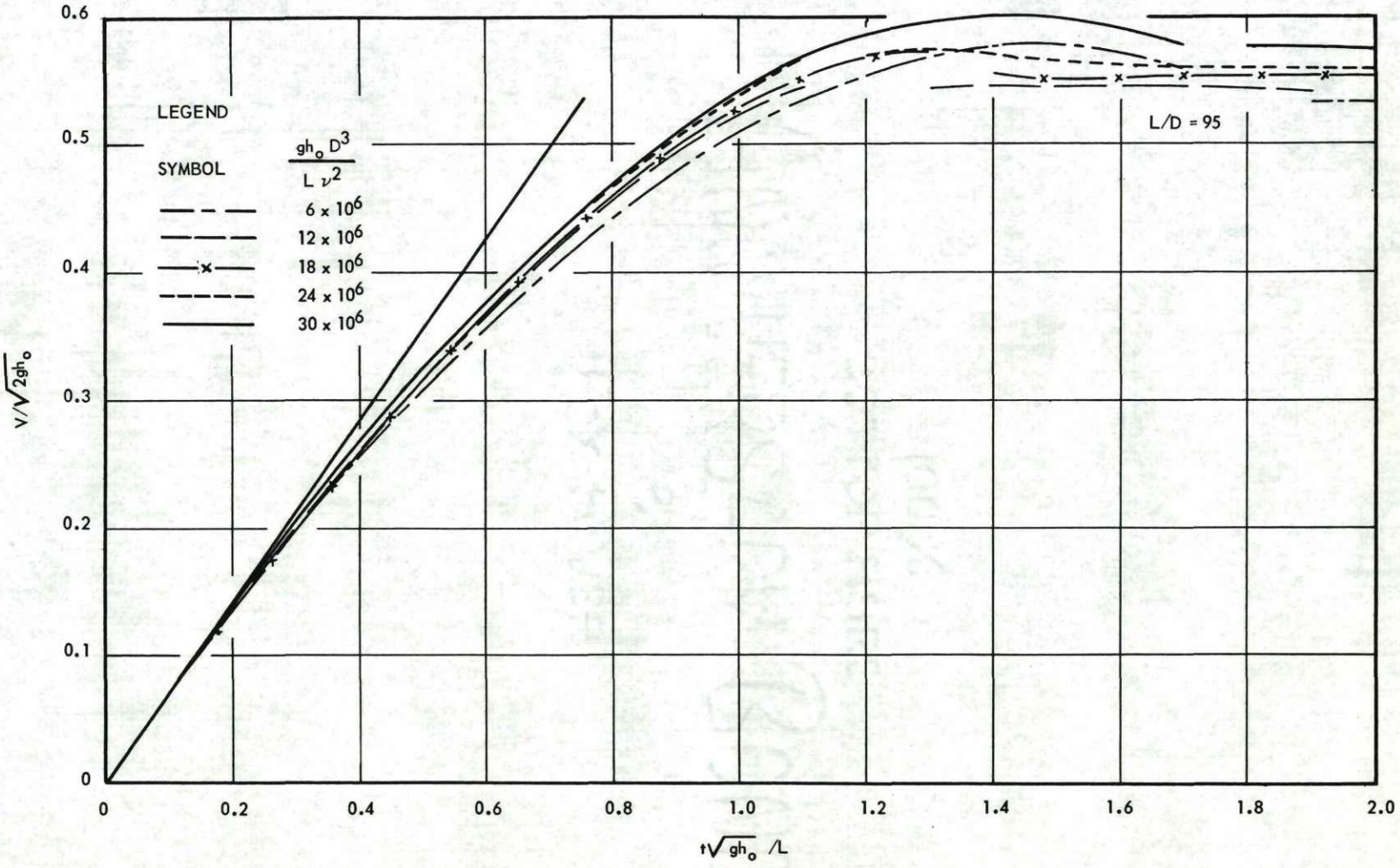

Figure 24. Mean velocity-time curves with L/D = 95.

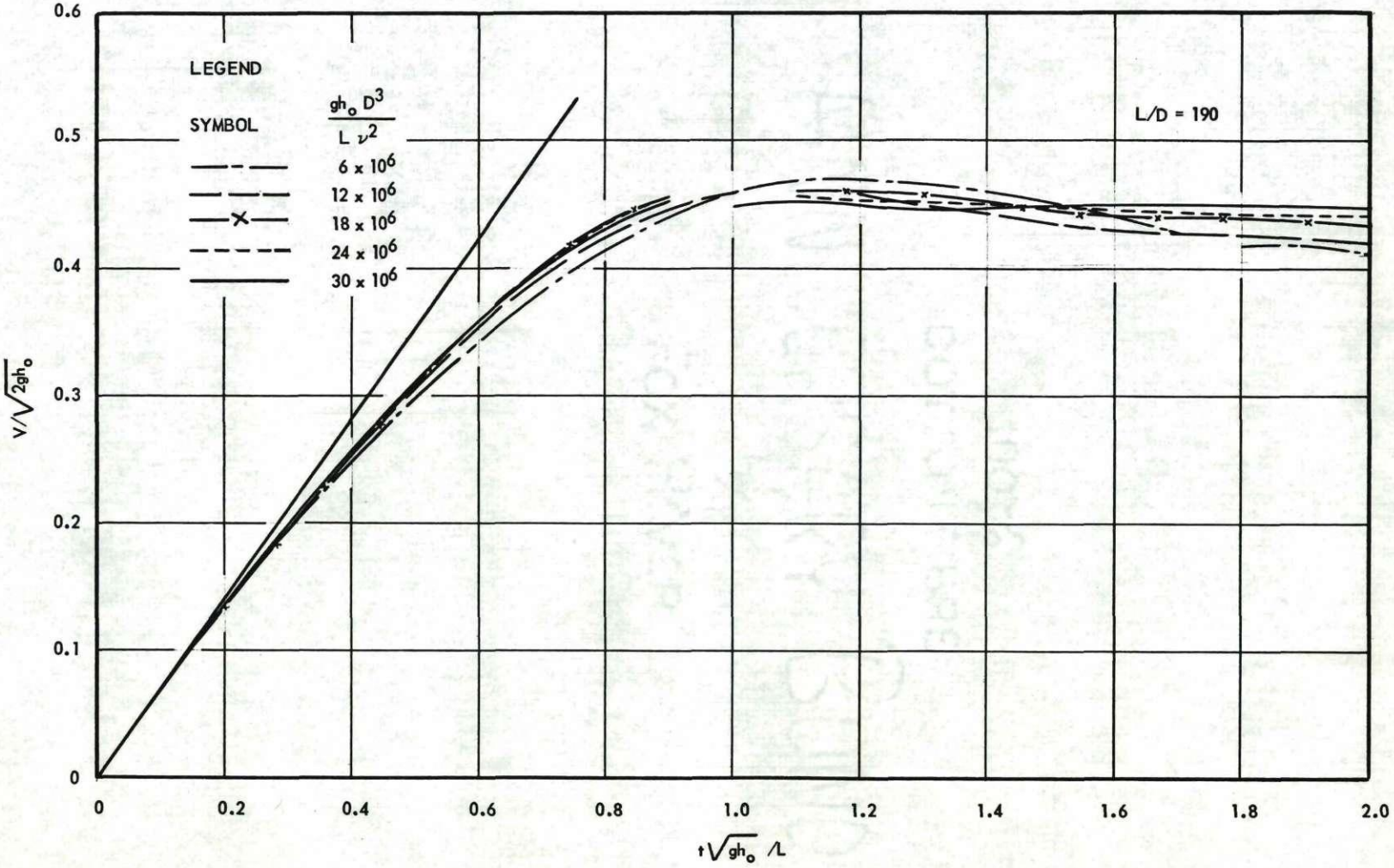

Figure 25. Mean velocity-time curves with L/D = 190.

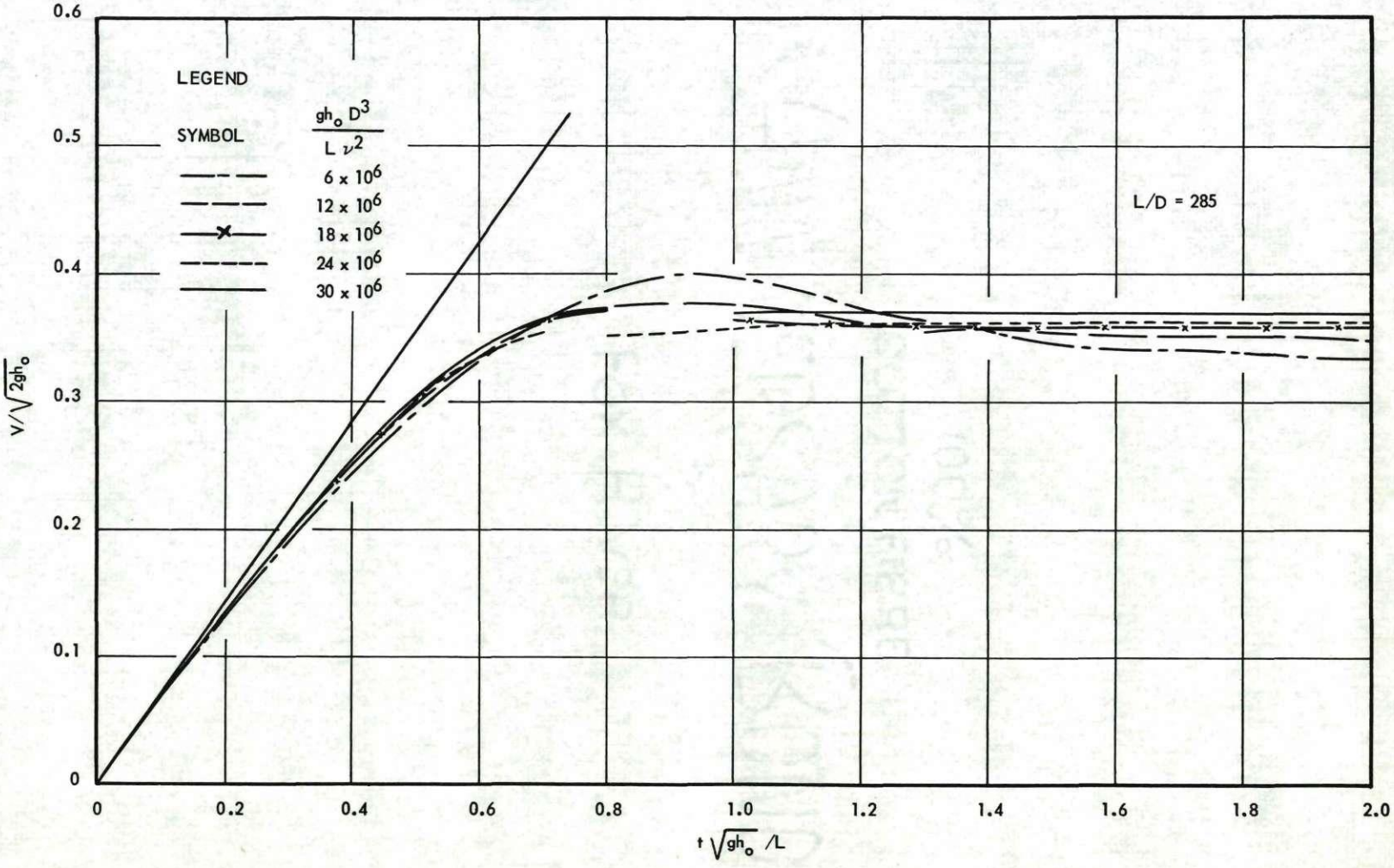

Figure 26. Mean velocity-time curves with L/D = 285.

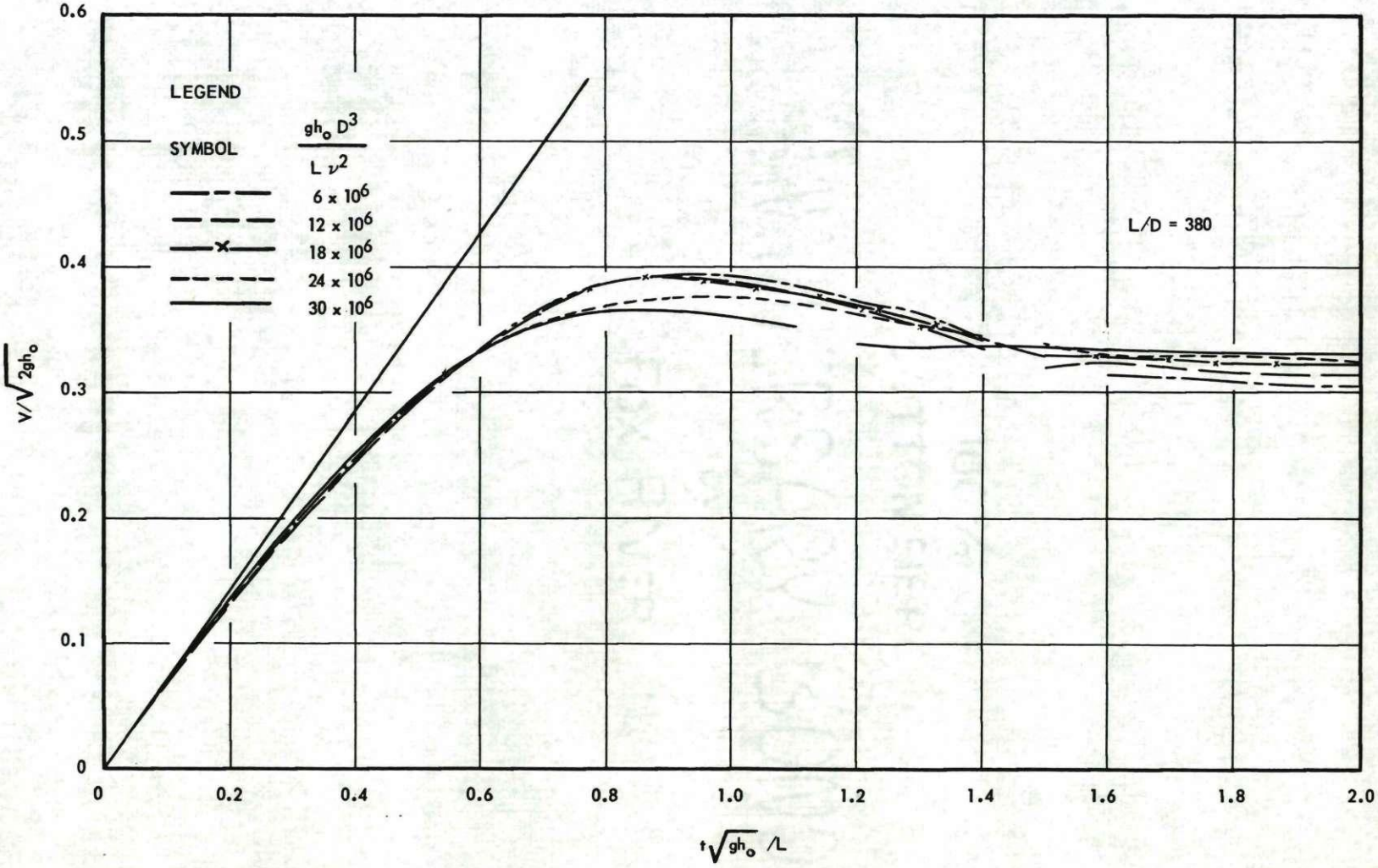

Figure 27. Mean velocity-time curves with L/D = 380.

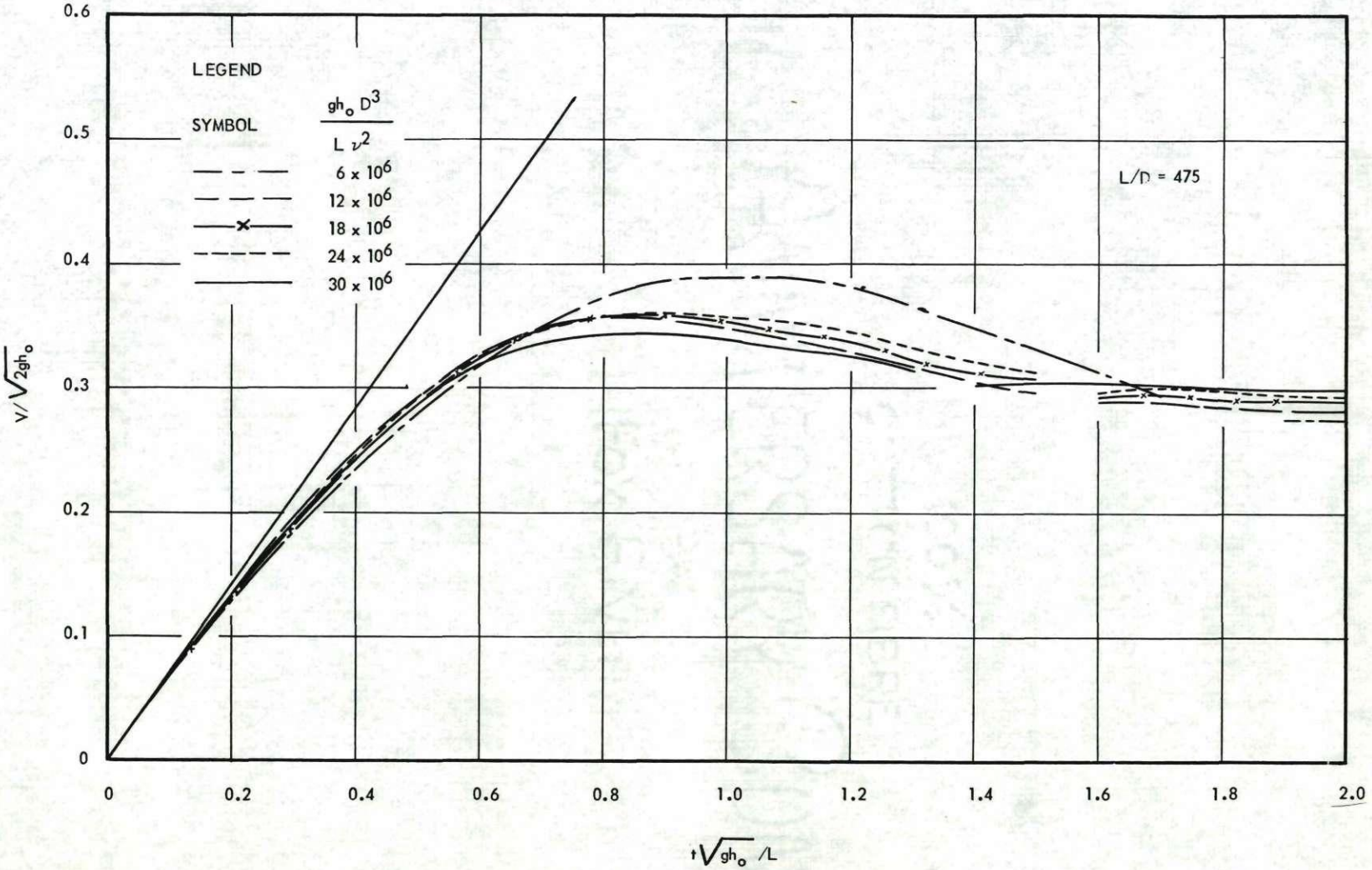

Figure 28. Mean velocity-time curves with L/D = 475.

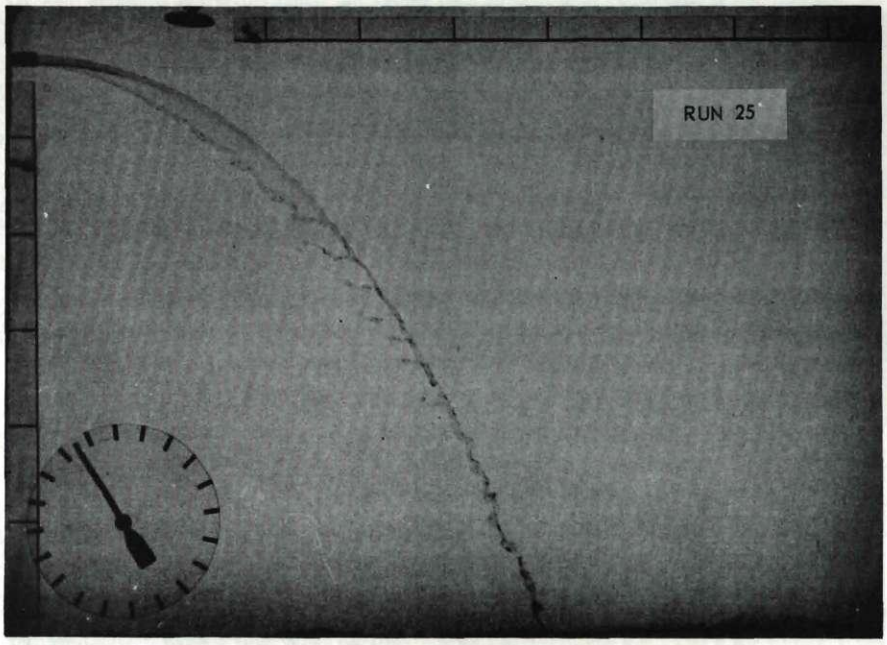

(a) T = 1.797 SEC.

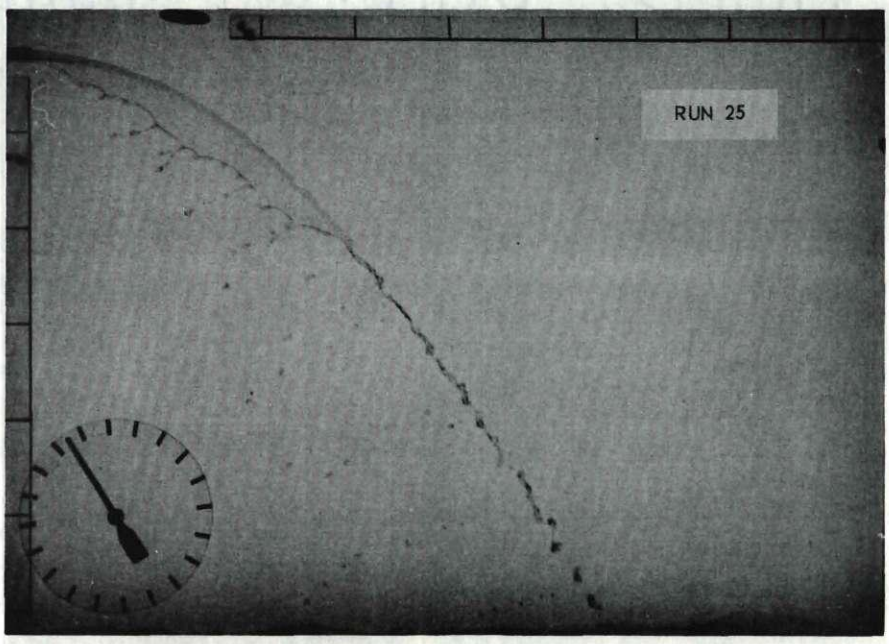

(b) T = 2.997 SEC.

Figure 29. Stages of jet separation.

The effect of jet separation on the observed velocity-time curves (Figs. 12 through 16) produced observed velocities of a magnitude greater than the actual case. Measurements of the jet coordinates were taken with respect to the inner core of the fluid. This inner core, due to incomplete transfer of linear momentum to the outer portion, had a linear momentum in excess of the mean linear momentum of the flow. Thus, the inner portion of the jet had a progressively higher value of observed velocity as the separation became more pronounced.

CHAPTER V

ANALYSIS OF RESULTS

In Chapter II, two solutions were obtained for flow establishment in a straight pipe. These solutions were obtained from the one-dimensional equation of motion by introducing gross assumptions as to the nature of the shear force. In this chapter a comparison of experimental results is made with the solutions obtained by one-dimensional analysis. Also, the results of the experimental program are analyzed with regard to application in engineering practice.

Comparison of results with the solutions obtained by one-dimensional analysis.--Equation (10) is a solution obtained by assuming the shear force is negligible. In the absence of any shear force, the piezometric head gradient is entirely utilized to accelerate the fluid mass. Initially the piezometric head gradient is h_o/L with the result that the initial acceleration is $(h_o/L)g$. The piezometric head gradient decreases with time since an increasing amount of energy is converted to kinetic energy as the fluid passes from the reservoir through the pipe inlet. At an infinite value of time the piezometric head gradient is zero, with the result that the acceleration is zero. Equation (10) is shown as the upper curve of Fig. 30.

The ideas employed in the derivation of Eq. (13) are those commonly utilized in engineering calculations involving unsteady flow in enclosed

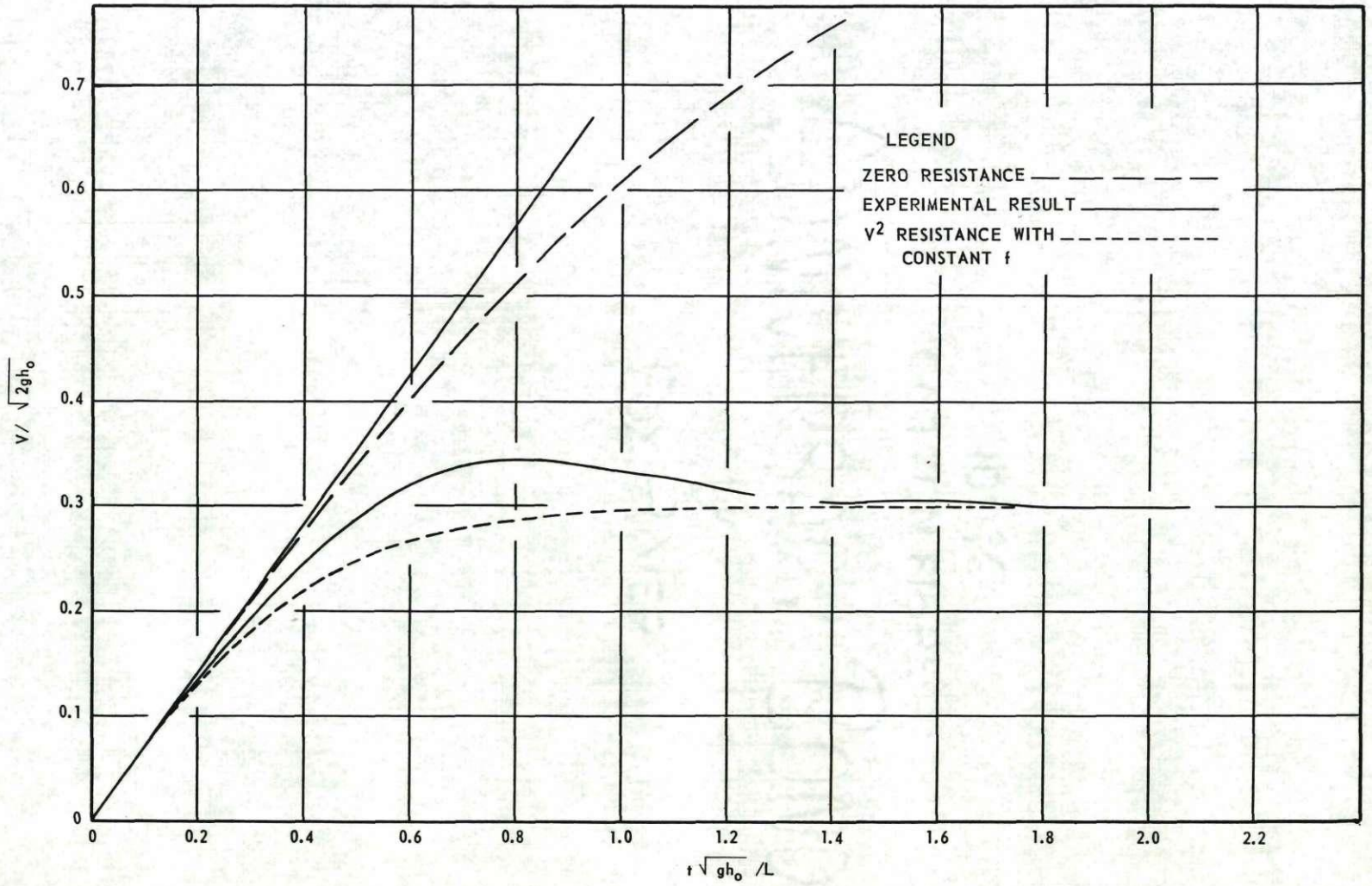

Figure 30. Comparison with solutions obtained by one-dimensional analysis.

conduits. In engineering practice unsteady flow in enclosed conduits occurs in lock culverts, in surge tanks and connected pipe lines, and in penstocks during hydraulic turbine tests, to cite a few examples. Invariably the analysis of these flows is predicated upon the use of the steady-state Darcy-Weisbach resistance equation for the unsteady flow. In many cases, the value of the Darcy-Weisbach resistance coefficient f is assumed constant throughout the entire range of velocities. In other cases, the value of f is computed for the instantaneous velocity value and the solution must be computed stepwise.

Equation (13) is a solution obtained by assuming a constant value of f. Initially the shear force is zero and the piezometric head gradient is utilized entirely to accelerate the fluid mass. The initial piezometric head gradient is h_o/L, with the result that the initial acceleration is $(h_o/L)g$. Again the piezometric head gradient decreases with time since an increasing amount of energy is converted to kinetic energy as the fluid passes from the reservoir through the pipe inlet. However, in this case, a portion of the piezometric head gradient is utilized to overcome the shear force. Consequently the acceleration will always be less than would be the case with no resistance of Eq. (10). This shear force continues to increase in magnitude until the piezometric head gradient is equal to the shear force. At this time the acceleration is zero. Theoretically an infinite time is required to reach this steady state. Equation (13) is the lower curve of Fig. 30. The constant value of f was computed from the terminal velocity of Run 29.

The experimental results of Run 29 are also shown on Fig. 30, which allows comparison of test results with Eqs. (10) and (13). Run 29

has been selected as being representative of the entire twenty-five runs. Initially the shear force is zero and the piezometric head gradient is entirely utilized to accelerate the fluid mass. The initial piezometric head gradient is h_o/L, with the result that the initial acceleration is $(h_o/L)g$. The piezometric head gradient decreases with time since an increasing amount of energy is converted to kinetic energy as the fluid passes from the reservoir through the pipe inlet. A portion of the piezometric head gradient is utilized to overcome the shear force. However, in this case, the shear force is initially far different from that visualized in the development of Eq. (13). The flow is initially laminar. The laminar boundary shear force is less than the corresponding turbulent boundary shear force. Consequently, as long as the flow is laminar, the acceleration of Run 29 will be greater than would be the case with turbulent resistance of Eq. (13). Also the acceleration of Run 29 will be less than would be the case with no resistance of Eq. (10). The differences in acceleration in the three cases are apparent at early values of time on Fig. 30.

The flow condition of Run 29 would continue as described above except for the instability of the laminar flow. At a value of $t\sqrt{gh_o}/L$ of approximately 0.6 a spot or region of turbulence is generated. This turbulent region increases in length as time passes. Until the turbulence appears at the end of the pipe at a time value of 1.35, both laminar and turbulent flow regions exist within the pipe. Thus, during the time interval $0.6 < t\sqrt{gh_o}/L < 1.35$ the turbulent region is continuously increasing and the laminar region is continuously decreasing. Since the turbulent

shear force is greater than the laminar shear force, the growing turbulent region results in a rapidly increasing shear force. Thus a much greater portion of the piezometric head gradient is utilized to overcome this rapidly increasing shear force. The result is that the acceleration is rapidly decreased. The acceleration is decreased to zero at a value of $t\sqrt{gh_o}/L$ of about 0.8 for Run 29. At this time the velocity is a maximum. This velocity is greater than the velocity determined from Eq. (13) because of the presence of laminar shear force at the early values of time. At this time, the time of zero acceleration, the piezometric head gradient is entirely utilized to overcome the shear force. However, the turbulent region is still expanding, with the result that the magnitude of the total boundary shear force is also increasing. Thus the magnitude of the total boundary shear force exceeds the total available piezometric head gradient beyond this point of zero acceleration. In such a case the flow must decelerate. The deceleration period of Run 29 is shown on Fig. 30 at values of $t\sqrt{gh_o}/L$ greater than 0.8. The appearance of the turbulence at the pipe outlet occurred at a value of $t\sqrt{gh_o}/L$ of 1.35. When turbulence appears at the pipe outlet, the turbulent flow region exists in the entire pipe length. For Run 29 the decleration is very small after the turbulent region exists in the entire pipe length.

Some general statements about flow establishment in any conduit can be made as a consequence of the previous analysis.

Cases of flow establishment.--Four possible velocity-time relationships may occur during flow establishment in a straight pipe. The particular relationship which occurs is a function of the time of turbulence inception,

of the rate of growth of the turbulent zone, and of the position of turbulence inception. The four relationships are distinguished by the time at which the flow within the pipe is completely turbulent. The four cases of velocity-time relationships are schematically illustrated on Fig. 31.

In Case I the time of turbulence inception is early and the rate of growth of turbulence is such that turbulence exists throughout the pipe before the velocity has equalled its terminal value. Thereafter, the establishment of flow is similar to Eq. (13) with a corresponding shift in time. Thus the time at which steady flow is essentially reached is less than the time indicated by Eq. (13). An experimental example of Case I is illustrated on Fig. 22 by the velocity-time function with the value of L/D equal to 285.

Case II, illustrated on Fig. 31, has a later time of turbulence inception than Case I with the same increment of time for turbulence growth. In Case II the flow is completely turbulent throughout the pipe as the velocity first reaches its terminal value. Thereafter, there will be no acceleration of the flow and the time of steady flow will be considerably less than that time indicated by Eq. (13). An experimental example of Case II is illustrated on Fig. 20 by the velocity-time function with the value of L/D equal to 95.

Case III, illustrated on Fig. 31, has a later time of turbulence inception than either of the previous cases but with the same increment of time for turbulence growth. In this case the time of complete turbulence is such that the velocity at this time is greater than its terminal value. Thereafter the turbulent flow will decelerate until the

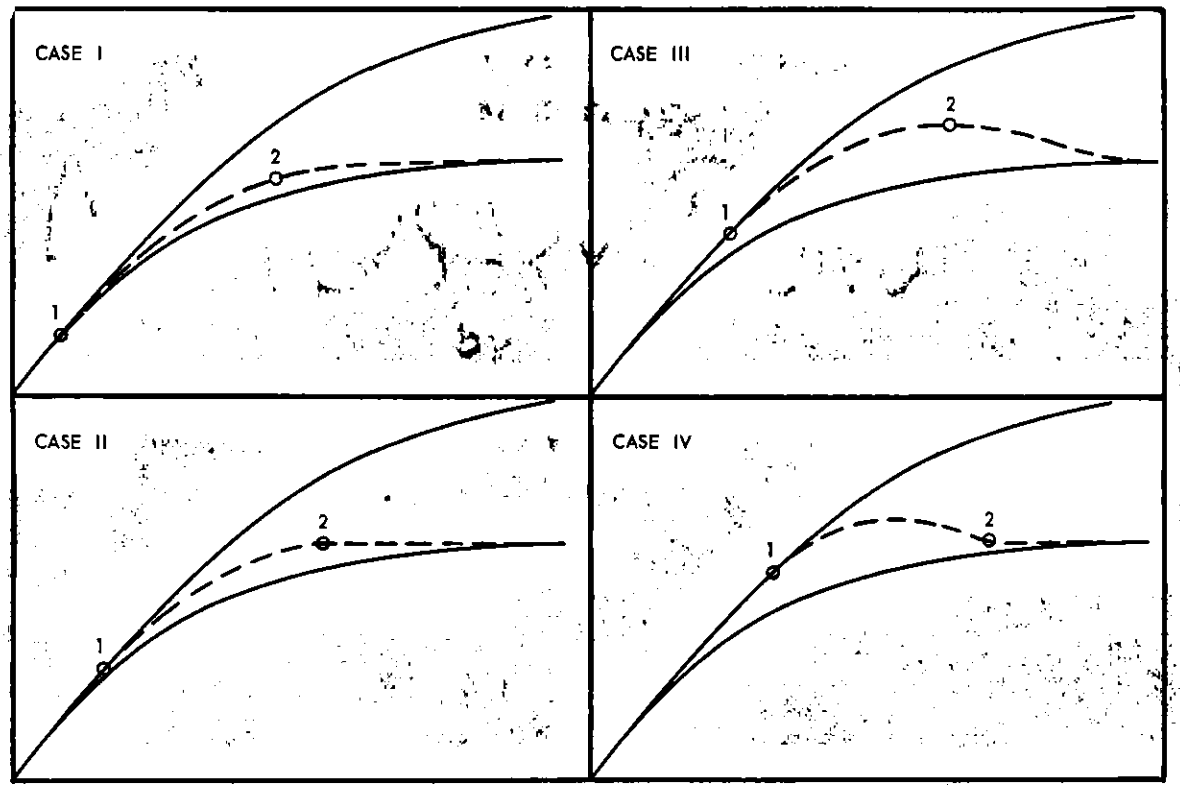

Figure 31. Schematic illustration of flow establishment cases.

terminal velocity is reached. The time at which essentially steady flow is reached is very unpredictable and may or may not exceed that predicted by Eq. (13). An experimental example of Case III is illustrated on Fig. 20 by the velocity-time function with the value of L/D equal to 190.

Case IV, illustrated on Fig. 31, with the same increment of time for turbulence growth, has the latest time of turbulence inception of all cases. In this case the latter-stage deceleration of the flow is essentially completed at the time of complete turbulence. Thereafter, minor decelerations may occur, but the time at which essentially steady flow is reached will generally be equal to or less than the time indicated by Eq. (13). Run 29 illustrated on Fig. 30 is an example of Case IV.

The different cases of flow establishment have been illustrated by noting only the change in time at which the inception of turbulence occurs. The time of growth of the turbulent zone in the pipe has been held at a constant value. Since the particular case of flow establishment occurring is a function of the time, place, and rate of growth of turbulent flow, each will be discussed separately in the following sections.

Time of turbulence inception.—The transition from laminar to turbulent flow has been studied in detail in Part II of this study. The results of Part II indicate that an inception of turbulence will occur when the boundary-layer Reynolds number reaches a certain value. The critical boundary layer $R_{\delta c}$ Reynolds number was determined to have the value of 5500. The boundary-layer Reynolds number is expressed as

$$R_{\delta} = \frac{v_c \delta}{\nu} \tag{41}$$

in which δ is the nominal boundary layer thickness and v_c is the core velocity or free-stream velocity in the pipe. Equation (41) can also be expressed in terms of the experimental parameters as

$$R_\delta = \sqrt{2}\ \frac{v_c}{V}\ n\ \frac{V}{\sqrt{2gh_o}} \sqrt{\frac{gh_o D^3}{L\upsilon^2}}\ \sqrt{\frac{L}{D}} \qquad (42)$$

where n is the dimensionless nominal boundary-layer thickness δ/r_o. The ratio v_c/V has been shown to be a function of n; therefore the product $\sqrt{2}\ n\ v_c/V$ is a function of n.

Assuming a constant value of L/D, the time rate of development of n may be assumed as equal for these purposes. (See Table III, Appendix.) The effect of an increase in the value of the head parameter $gh_oD^3/L\upsilon^2$ would reduce the value of the product, $\sqrt{2}\ n\ v_c/V(V/\sqrt{2gh_o})$. Since n becomes essentially a constant immediately after its initial rapid increase (Table III), the end result would be a reduction in the value of the velocity parameter at which the critical boundary-layer Reynolds number would occur. From Figs. 24 through 28 it can be seen that for a constant L/D, the values of $V/\sqrt{2gh_o}$ at early times are essentially equal for various values of $gh_oD^3/L\upsilon^2$. Therefore a reduction in $V/\sqrt{2gh_o}$ would necessarily result in a reduction in the time at which the critical value of the boundary-layer Reynolds number is attained.

Thus, an increase in the value of the head parameter with a constant value of L/D would result in a reduction in the time of turbulence inception. This can be readily seen from a tabulation of the earliest times at which turbulence is observed. These times are found in Part II

of this study.

The time at which turbulence is first observed is not always the time of inception, for the turbulence is observed at the piezometers only. The inception could occur between the piezometers with a resulting time lag before observance. However, the effects of the head parameters are apparent from this data. The trend can also be seen, although not as forcefully, on the mean velocity-time curves of Figs. 25 through 28. Figure 24 is here omitted since the first observance of turbulence was at the end of the pipe or when complete turbulence existed in the pipe.

Assuming a constant value of $gh_o D^3/L\,\upsilon^2$, with all the previous assumptions regarding n, an increase in the value of L/D also reduces the value of $V/\sqrt{2gh_o}$ at which the critical boundary-layer Reynolds number would occur. However, Figs. 19 through 23 show that an increase in the value of L/D reduces the value of $V/\sqrt{2gh_o}$ at any given time, which tends to compensate for the variation in the time of inception. A tabulation of the earliest times at which turbulence is seen from Part II reveals no systematic variation in the time of turbulence inception with a variation in the value of L/D. Thus it is believed from the experimental results that variation in the value of L/D has only minor effects on the times of turbulence inception.

Rate of turbulence growth and position of turbulence inception. Figure 32 is a schematic sketch of a typical flow establishment in which $\Delta t\ \sqrt{gh_o}/L$ is the dimensionless time increment from the inception of turbulence to complete turbulence in the pipe. The increment of time Δt

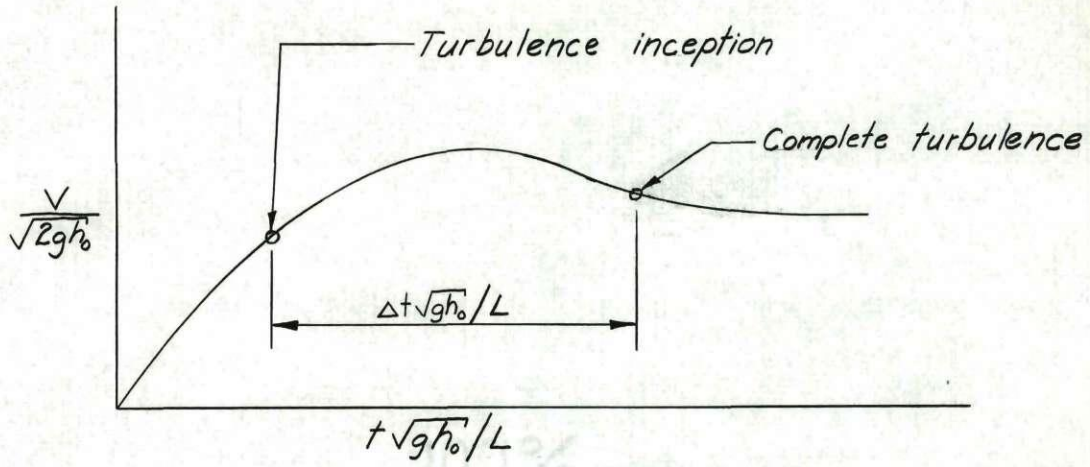

Fig. 32. Typical flow establishment

is dependent upon the rate of turbulence growth and the distance through which the growth must take place. From the results of Part II of this study, the rate of turbulence growth V^* may be presented as

$$\frac{V^*}{V} = 1.35 \tag{43}$$

The distance through which the growth takes place L^* is the distance from the position of turbulence inception to the pipe outlet. Replacing V^* in Eq. (43) by L^* and Δt, Eq. (43) reduces to

$$\frac{L^*}{\Delta t} = 1.35\ V \tag{44}$$

Multiplying Eq. (44) by $\sqrt{2gh_o}/L$ and rearranging, leaves

$$\frac{L^*/L}{\sqrt{2}\ \ 1.35\ V/\sqrt{2gh_o}} = \frac{\Delta t\ \sqrt{gh_o}}{L} \tag{45}$$

The left side of Eq. (45) is composed of the velocity parameter and a dimensionless length of the turbulent growth zone. The right side is the

dimensionless time increment for the complete growth of the turbulent zone. Since for a constant value of L/D the velocity parameters are essentially equal, the time increment for turbulent growth is a direct function of the position of turbulence inception. Therefore the position of turbulence inception is of great importance in determining the time of growth and the particular case of flow establishment which results. It was determined in Part II of this study that the position of inception was not constant nor was it a function of any of the experimental parameters.

The fluctuation of the position of turbulence inception can possibly be explained by the critical boundary-layer Reynolds number. During early times there exist two regions of boundary-layer growth. One is the inlet region where the nominal boundary layer thickness is growing both with distance from the inlet and with time. The other region lies downstream from the inlet region. In this region the layer thickness δ is growing with time alone and is a constant value downstream from the inlet region at any given time. Thus, due to the inlet effects on δ, the nominal thickness below the inlet region is always greater than the thickness within the inlet region. Hence, the critical boundary-layer Reynolds number will occur instantaneously at all points downstream from the inlet region. Thus the turbulence inception could occur at any point in the pipe below the inlet region. However, since in the experimental program the flow is initially disturbed at the inlet by the band of sand grains, it is probable that turbulence inception would occur just below or at the lower extremity of the inlet region.

An increase in the value of L/D will not change the fact that the turbulence inception could occur at any point below the inlet region, but it is probable that the ratio L^*/L will approach a value of one for the longer pipes. As the value of L^*/L approaches the limit of one, the time for complete turbulent growth approaches its maximum value. Thus, there will be an increase in the time for complete turbulent growth with an increase in the value of L/D.

Figures 19 through 23 are illustrated at a constant value of the head parameter to demonstrate the effects of variation in L/D. From the previous analysis it has been seen that the time of turbulence inception is generally constant for a constant value of $\frac{gh_oD^3}{L\upsilon^2}$ and for any value of L/D. Thus the cases of flow establishment resulting in Figs. 19 through 23 are determined by the increments of time required for turbulence growth. From Eq. (45) it is apparent that relatively low values of $V/\sqrt{2gh_o}$ would result in high values of $t\sqrt{gh_o}/L$. Since the values of L/D which are high produce relatively lower values of $V/\sqrt{2gh_o}$, the time for turbulence growth will be directly proportional to the value of L/D. Also, from the previous discussion on the position of turbulence inception, the longer the pipe, the higher the value of L^*/L. Therefore the relative effects of long pipes produce later times of complete turbulence. Thus for long pipes the case of flow establishment would be predominantly Case IV. Table IV in the Appendix is a tabulation of all experimental results and their classifications.

Analysis of results with regard to engineering applications.—A qualitative analysis encompassing a wide range of variables found in engineering

practice was made to indicate the effect of these variables. In order for the results of this study to be applied to a qualitative analysis of engineering applications, several assumptions must be made as to the events which take place in a flow establishment. First, there must be an inception of turbulence within the pipe. Second, this spot or region of turbulence must generate in only one position in the pipe with a subsequent downstream growth. Third, the trends indicated by the experimental results must continue for extrapolations beyond the values of the experimental parameters.

The time of turbulence inception occurring in engineering applications was determined to be most affected by a variation in the pipe diameter, since the head parameter contains the third power of the diameter. An increase in the pipe diameter reduces the time of turbulence inception. Thus the time of turbulence inception in a 1-foot diameter pipe would be less than the time in the 1/2-inch diameter pipe used in these experiments. The results of the qualitative analysis indicate that the inception of turbulence will occur at very early times, that is, at values of $t\sqrt{gh_o}/L$ of 0.15, 0.10, and so forth. A reduction in the time of inception can also be expected due to the effects of inlets found in engineering applications. For example, the extreme case of a square-edged inlet would cause separation with a contracted flow region just downstream from the inlet. The subsequent downstream expansion of the flow would result in high instability within the fluid. This in turn would reduce the time at which the transition from laminar to turbulent flow would occur.

The effect of inlets found in engineering practice could also tend to control the position of turbulence inception. It is believed that the great instability within the fluid just downstream from the inlet would certainly result in a turbulent inception at that point. If this occurs, the value of L^*/L in Eq. (45) would be a maximum. Thus, the time for complete turbulent growth would be a function of $V/\sqrt{2gh_o}$. Since the longer pipes result in lowered values of $V/\sqrt{2gh_o}$, at a constant value of the head parameter, the time for turbulence growth would be longer.

In summing up the results of the qualitative analysis, the reduction in the time of turbulence inception in engineering applications is more than offset by the increase in the time of turbulence growth. Thus, the case of flow establishment which dominates in the engineering applications is believed to be Case IV, with Case III possibly appearing in the shorter pipes, that is, L/D is equal to 95, 190, and so forth. Due to the early times of turbulence inception found in engineering practice, it is believed that at early times the velocity-time function will be nearer to Eq. (13) than to the empirical results.

In the solution of Eq. (13), the effect of a variation in f, the Darcy-Weisbach coefficient, over the total range of velocities was neglected and a constant value of f was utilized. This assumption has been commonly employed in engineering calculations involving unsteady flow. A variation commonly employed in this procedure is to determine a value of f for a small increment of time, thereby utilizing step-computation methods and the effects of a change in the Reynolds number for each step.

This method of solution would have a slight effect on Eq. (13) as presented in Fig. 30. The effect would tend to lower the curve slightly at early times. This method results in a more accurate solution than Eq. (13) if turbulent flow exists throughout the pipe for values of time greater than zero. However, since beginning flow in a pipe is in the laminar state, the actual velocity-time relationship will lie above the method of solution of completely turbulent flow which employs the effects of a variation in f with the Reynolds number. Since at early times Eq. (13) also lies above the method of solution with varying f, Eq. (13) is believed to be a closer approximation at early times to the actual velocity-time relationships encountered in engineering applications.

In summing up the analysis of the results, several questions still remain. The most important of these is the seemingly uncorrelated position at which the inception of turbulence occurred. There appeared to be no systematic relationship between the position and the experimental parameters. It could be erroneously concluded that there is no relationship which controls the position of turbulence except for the fact that the position of turbulence was the same when the experimental run was duplicated. Thus, the conclusion which must be reached is that the experimental parameters used were insufficient to control the point of turbulence inception.

Also of importance in the establishment of flow in cases found in engineering practice is the fact that turbulence inception could possibly occur at two or more points within the pipe. This occurrence is quite

feasible in a rough pipe, for the pipe roughness could produce vibrations similar to those caused by the sand grains in the inlet of the experiment. Due to the smooth pipe used in the experiment, all vibrations originated from the sand grains in the inlet.

Part II of this study reveals that once a spot of turbulence is generated within the pipe, the upstream vibrations are effectively blocked from the downstream fluid. Thus, only one zone of turbulence is generated in a smooth pipe, with subsequent growth downstream. Whereas, in a rough pipe, two or more or even an infinite number of zones may be generated at once. If the fluid in the pipe experienced an infinite number of turbulence inception zones, the flow, of course, would be completely turbulent in an instant, with the result that a highly developed Case I flow establishment would occur, approximating Eq. (13). If only two or more zones generated, the length of growth L^* in Eq. (45) would be the distance from the outlet to the position of the zone nearest the outlet. This is due to the almost instantaneous upstream growth of turbulence which is cited in Part II of this study. Since the increment of time for complete turbulent growth will be greatly foreshortened by decreasing L^*, Case I or possibly Case II may occur as the flow establishment.

CHAPTER VI

CONCLUSIONS

1. For turbulent flow conditions, the method of obtaining mean velocities by jet photography entails only an assumption of a velocity distribution.

2. For laminar flow conditions, the method of jet photography for obtaining mean velocities requires that a velocity distribution be assumed, that pressure measurements be obtained at various points along the pipe, and that there be no separation of the issuing laminar jet.

3. Separation of the laminar jet occurs when the value of δ/r_o becomes greater than 0.65.

4. The use of step computations with a variable value of the Darcy-Weisbach f is unwarranted. In engineering computations the use of a constant value of f is sufficiently accurate. Neither computation is physically correct because of the initial laminar flow.

5. The exact variation of velocity with respect to time during flow establishment is a function of the time of turbulence inception, the rate of growth of the turbulent region, and the position of turbulence inception.

6. The experimental parameters utilized in the experiment were sufficient to insure similarity in regard to the time of turbulence inception and the rate of growth of the turbulent region. Since the position of

turbulence inception is apparently random, the experimental parameters are not sufficient to insure exact similarity in regard to the variation of velocity with respect to time during flow establishment.

References

[1] Laufer, John. "The Structure of Turbulence in Fully Developed Pipe Flow," United States National Advisory Committee for Aeronautics, Report 1174, 1954.

[2] Sandborn, Virgil A. "Experimental Evaluation of Momentum Terms in Turbulent Pipe Flow," United States National Advisory Committee for Aeronautics, Technical Note 3266, January, 1955.

[3] Rich, George B. Hydraulic Transients. New York: The McGraw-Hill Book Company, 1951.

[4] Valensi, J., and Clarion, C. "Mouvement oscillatoire d'un liquide visqueux et pesant dans un tube en U; photographie du profil des déplacements; mise en évidence de la turbulence," Comptes Rendus des Séances de l'Académie des Sciences, Vol. 226, 1948, p. 554.

[5] Clarion, C. "Sur l'amortissement des petites oscillations d'un liquide pesant et visqueux dans un tube en U," Comptes Rendus des Séances de l'Academie des Sciences, Vol. 230, 1950, p. 1926.

[6] Yamada, H. and Taneda, S. "Note on the Liquid Motion in a U-tube," Reports of the Research Institute for Fluid Engineering, Kyushu University, Japan, Vol. VII, September, 1950, p. 1.

[7] Christopherson, D. G., et al. "Oscillatory Motion of a Fluid Along a Circular Tube," Proceedings of the Royal Society of London, Series A, Vol. 168, November, 1938, p. 351.

[8] Jones, D. B. "Measurement of Fluid Resistance in Oscillatory Unsteady Flow in a Smooth Pipe," Unpublished Master's thesis, State University of Iowa, August, 1954, 54p.

[9] Crausse, E. "Contribution à l'étude expérimentale de phénomènes transitoires et de phénomènes périodiques se produisant dans les liquides en mouvement," Publication Scientifiques et Techniques du Ministère de l'Air, No. 95, 1936.

[10] Daily, James W., and Deemer, Kenneth C. "The Unsteady-Flow Water Tunnel at the Massachusetts Institute of Technology," Transactions of the American Society of Mechanical Engineering, Vol. 76, January 1954, p. 87.

[11] Szymanski, Piotr. "Quelques solutions exactes des équations de l'hydrodynamique du fluide visqueux dans le cas d'un tube cylindrique," Journal de Mathématiques Pures et Appliquées, Series 9, Vol. 11, 1932, p. 67-107.

[12] Langhaar, Henry L. "Steady Flow in the Transition Length of a Straight Tube," Journal of Applied Mechanics, Vol. 9, No. 1, March, 1942, p. A55-A58.

[13] Goldstein, S. (editor). Modern Developments in Fluid Dynamics, Vol. I, Oxford: The Clarendon Press, 1938, p. 299-304.

[14] Prandtl, L., and Tietjens, O. G. Applied Hydro- and Aeromechanics. Tranlated by J. P. Den Hartog. New York: The McGraw-Hill Book Company, 1934, p. 40-74.

APPENDIX

TABULATED EXPERIMENTALLY DETERMINED VALUES

Table I. Range of Experiment

Run No.	L/D	$\frac{gh_o D^3}{L\upsilon^2}$ (x10^{-6})
4	95.08	30.21
5		24.04
6		18.06
7		12.04
8		6.03
10(3)	190.16	5.99
*10a		6.00
9(2)		12.02
11		17.92
*11a		18.01
*11b		17.94
12		23.87
*12b		24.14
13		29.87
*13a		29.89
*13b		30.01
15	285.20	5.98
16		11.99
*16a		11.99
17		18.03
18		24.02
19		30.00
20	380.28	5.99
*20a		5.98
*20b		5.96
21		11.97
*21a		11.98
22		17.97
*22a		17.91

(continued)

Table I. Range of Experiment (continued)

Run No.	L/D	$\frac{gh_o D^3}{L\upsilon^2}$ $(x10^{-6})$
23	475.34	23.88
*23a		23.98
*23b		23.96
24		30.30
*24a		29.89
25		5.98
*25a		5.97
26		11.95
*26a		12.00
27		18.00
*27a		17.98
*27b		17.97
*27c		17.96
*27d		17.94
*27e		17.92
*27f		17.92
28		23.92
*28a		24.00
29		29.85
*29a		29.97

*Denotes runs repeated for pressure evaluation.

Table II. Pipe Geometry

Micrometer measurements of the pipe diameter

Pipe No.	$\bar{L}$ (ft.)	Numbered End of Pipe D_1* (in.)	D_2* (in.)	Ave. D (in.)	Opposite End of Pipe D_1* (in.)	D_2* (in.)	Ave. D (in.)
1	4.310	0.544	0.543	0.5435	0.543	0.543	0.543
2	4.310	0.545	0.543	0.544	0.545	0.544	0.5445
3	4.308	0.545	0.543	0.544	0.544	0.544	0.544
4	4.310	0.544	0.542	0.543	0.544	0.545	0.5445
5	4.309	0.545	0.543	0.544	0.545	0.545	0.545
				Mean D = 0.5437			Mean D = 0.5442

*D_1 and D_2 are orthogonal diameters.

Weight-volume determination of the pipe diameters

Pipe No.	Dry Weight of Pipe (gm.)	Weight of Pipe + Water (gm.)	Weight of Water (gm.)	Water Temp. (°C)	Vol. of Water ($cm.^3$)	$\bar{L}$ (cm)	Avg. D (cm)	Avg. D (in)
1	2427	2622	195	24.5	195.5	131.3	1.38	0.543
2	2420	2619	199	25.7	199.5		1.39	0.547
3	2423	2623	200	25.7	200.5		1.39	0.547
4	2427	2622	195	25.6	195.5		1.38	0.543
5	2410	2605	195	25.2	195.5		1.38	0.543
				Avg. Temp. = 25.3°C				Mean D = 0.5446

The mean diameter of all pipes was assumed to be 0.544 inch.

Table III. Empirical Results of n-t Relationship

Run No.	L/D	$\frac{gh_oD^3}{L\upsilon^2}$ ($\times 10^{-6}$)	$\frac{t\sqrt{gh_o}}{L}$	Method	$\frac{\delta}{r_o}$
29	475	30	0.20	III	0.10
			0.30		0.10
			0.40		0.13
			0.50		0.14
			0.60		0.18
			0.70		0.20
			0.80		0.24
			0.90		0.24
			1.00		0.29
			0.65	II	0.29
			0.62		0.29
			0.72		0.31
			1.06		0.37
			1.38	I	0.43
28	475	24	0.20	III	0.16
			0.40		0.11
			0.60		0.19
			0.80		0.23
			1.00		0.26
			1.20		0.30
			0.66	II	0.18
			0.64		0.15
			0.96		0.34
			1.27		0.37
			1.60	I	0.59
27	475	18	0.20	III	0.11
			0.30		0.13
			0.40		0.17
			0.50		0.18
			0.60		0.24
			0.70		0.29
			0.80		0.29
			0.70	II	0.20
			0.64		0.18
			0.96		0.34*
			1.26		0.41*
			1.58	I	0.72*

(continued)

Table III. Empirical Results of n-t Relationship
(continued)

Run No.	L/D	$\frac{gh_o D^3}{L\upsilon^2}$ ($\times 10^{-6}$)	$\frac{t\sqrt{gh_o}}{L}$	Method	$\frac{\delta}{r_o}$
26	475	12	0.20	III	0.21
			0.30		0.22
			0.40		0.15
			0.50		0.15
			0.60		0.19
			0.70		0.24
			0.80		0.25
			0.90		0.33
			0.72	II	0.23
			0.68		0.31
			0.98		0.34
			1.29		0.47*
			1.57	I	0.89*
25	475	6	0.20	III	0.26
			0.30		0.28
			0.40		0.27
			0.50		0.40
			0.60		0.35
			0.70		0.40
			0.80		0.42
			0.76	II	0.22
			1.04		0.34*
			1.29		0.39*
			1.57		0.42*
			1.85	I	1.00*
24	380	30	0.20	III	0.10
			0.30		0.11
			0.40		0.11
			0.50		0.11
			0.60		0.14
			0.70		0.18
			0.80		0.14
			0.66	II	0.14
			0.68		0.16
			0.80		0.19
			1.19	I	0.34

(continued)

Table III. Empirical Results of n-t Relationship
(continued)

Run No.	L/D	$\frac{gh_o D^3}{L\nu^2}$ $(x10^{-6})$	$\frac{t\sqrt{gh_o}}{L}$	Method	$\frac{\delta}{r_o}$
23	380	24	0.20	III	0.09
			0.30		0.09
			0.40		0.16
			0.50		0.23
			0.60		0.16
			0.70		0.15
			0.80		0.23
			0.90		0.30
			1.00		0.35
			0.74	II	0.25
			1.09		0.28
			1.48	I	0.46
22	380	18	0.20	III	0.12
			0.30		0.11
			0.40		0.12
			0.50		0.13
			0.60		0.18
			0.70		0.16
			0.80		0.23
			0.90		0.25
			1.00		0.27
			1.10		0.33
			0.80	II	0.26
			1.11		0.31
			1.48	I	0.48
21	380	12	0.20	III	0.12
			0.30		0.15
			0.40		0.16
			0.50		0.16
			0.60		0.15
			0.70		0.20
			0.80		0.26
			0.90		0.22
			1.00		0.24
			1.10		0.30

(continued)

Table III. Empirical Results of n-t Relationship
(continued)

Run No.	L/D	$\frac{gh_o D^3}{L\upsilon^2}$ $(x10^{-6})$	$\frac{t\sqrt{gh_o}}{L}$	Method	$\frac{\delta}{r_o}$
			0.80	II	0.26
			1.11		0.31
			1.49	I	0.62
20	380	6	0.20	III	0.17
			0.30		0.18
			0.40		0.22
			0.50		0.26
			0.60		0.26
			0.70		0.24
			0.80		0.25
			0.90		0.31
			1.00		0.45
			0.80	II	0.25
			0.88		0.20
			1.19		0.35*
			1.58	I	0.69*
19	285	30	0.20	III	0.09
			0.30		0.10
			0.40		0.09
			0.50		0.09
			0.60		0.09
			0.70		0.09
			0.91	I	0.23
18	285	24	0.20	III	0.09
			0.30		0.09
			0.40		0.09
			0.50		0.11
			0.60		0.09
			0.75	I	0.12
17	285	18	0.20	III	0.09
			0.30		0.10
			0.40		0.10
			0.50		0.12
			0.60		0.09
			0.92	I	0.28

(continued)

Table III. Empirical Results of n-t Relationship
(continued)

Run No.	L/D	$\frac{gh_o D^3}{L\nu^2}$ $(x10^{-6})$	$\frac{t\sqrt{gh_o}}{L}$	Method	$\frac{\delta}{r_o}$
16	285	12	0.20	III	0.11
			0.30		0.14
			0.40		0.14
			0.50		0.12
			0.60		0.15
			0.70		0.23
			0.71	II	0.26
			1.28	I	0.46
15	285	6	0.20	III	0.15
			0.30		0.17
			0.40		0.20
			0.50		0.29
			0.60		0.41
			0.78	II	0.29
			0.74		0.30
			1.36	I	0.56
13	190	30	0.20	III	0.09
			0.30		0.09
			0.40		0.11
			0.50		0.11
			0.60		0.11
			1.00	I	0.20
12	190	24	0.20	III	0.11
			0.30		0.11
			0.40		0.12
			0.50		0.12
			0.60		0.13
			1.03	I	0.20
11	190	18	0.20	III	0.08
			0.30		0.11
			0.40		0.15
			0.50		0.15
			0.60		0.14
			0.70		0.11
			1.03	I	0.20

(continued)

Table III. Empirical Results of n-t Relationship
(continued)

Run No.	L/D	$\frac{gh_oD^3}{L\upsilon^2}$ $(x10^{-6})$	$\frac{t\sqrt{gh_o}}{L}$	Method	$\frac{\delta}{r_o}$
9(2)	190	12	0.20	III	0.12
			0.30		0.13
			0.40		0.15
			0.50		0.17
			0.60		0.17
			0.70		0.15
			1.13	I	0.33
10(3)	190	6	0.20	III	0.13
			0.30		0.18
			0.40		0.21
			0.50		0.24
			0.60		0.27
			0.70		0.28
			1.76	I	0.65
4	95	30	1.75	I	0.33
5	95	24	1.15	I	0.12
6	95	18	1.42	I	0.28
7	95	12	1.26	I	0.28
8	95	6	1.87	I	0.41

*Based upon data after jet separation has occurred. Refer to p. 58 for explanation.

Table IV. Tabulation of Experimental Runs
by Cases of Flow Establishment

$\frac{gh_o D^3}{L\nu^2}$	L/D				
	475	380	285	190	95
30×10^6	IV	IV	II	II	IV
24×10^6	IV	IV	I	III	III
18×10^6	IV	IV	II	III	IV
12×10^6	IV	IV	IV	III	II
6×10^6	IV	IV	III	III	IV